

Resolving temperature **limitation** on spring productivity in an evergreen conifer forest using a model-data fusion framework

Stephanie G. Stettz¹, Nicholas C. Parazoo², A. Anthony Bloom², Peter D. Blanken³, David R. Bowling⁴, Sean P. Burns^{3,5}, Cédric [Bacour](#)⁶, Fabienne [Maignan](#)⁷, Brett Raczka⁵, Alexander J. [Norton](#)², Ian [Baker](#)⁸, Mathew [Williams](#)^{9,10}, Mingjie [Shi](#)¹¹, Yongguang [Zhang](#)¹², Bo Qiu¹²

¹Department of Earth System Science, University of California Irvine, Irvine, California, USA

²Jet Propulsion Laboratory, California Institute of Technology, Pasadena, California, USA

³Department of Geography, University of Colorado Boulder, Boulder, Colorado, USA

⁴[School of Biological Sciences, University of Utah, Salt Lake City, Utah, USA](#)

⁵[National Center for Atmospheric Research, Boulder, Colorado, USA](#)

⁶NOVELTIS, 153 rue du Lac, 31670 Labège, France

⁷Laboratoire des Sciences du Climat et de l'Environnement, LSCE/IPSL, CEA-CNRS-UVSQ, Université Paris-Saclay, Gif-sur-Yvette, France

⁸Cooperative Institute for Research in the Atmosphere, Colorado State University, Fort Collins, Colorado, USA

⁹School of GeoSciences and National Centre for Earth Observation, University of Edinburgh, Edinburgh, UK

¹⁰National Centre for Earth Observation, Edinburgh EH9 3FF, Edinburgh, UK

¹¹[Pacific Northwest National Laboratory, 902 Battelle Blvd, Richland, WA 99354](#)

¹²International Institute for Earth System Sciences, Nanjing University, Nanjing, Jiangsu Province, China

*Correspondence to: Stephanie Stettz (sstettz@uci.edu)

Abstract

[The flow of carbon through terrestrial ecosystems and the response to climate is a critical but highly uncertain process in the global carbon cycle.](#) However, with a rapidly expanding array of in situ and satellite data, there is an opportunity to improve our mechanistic understanding of the carbon (C) cycle's response to land use and climate change. Uncertainty in temperature **limitation** on productivity poses a significant challenge to predicting the response of ecosystem carbon fluxes to a changing climate. Here we diagnose and quantitatively resolve environmental limitations on growing season onset of gross primary production (GPP) using nearly two decades of meteorological and C flux data (2000-2018) at a subalpine evergreen forest in Colorado, USA. We implement the CARDAMOM model-data fusion network to resolve the temperature sensitivity of spring GPP. To capture a GPP temperature **limitation**—a critical component of integrated sensitivity of GPP to temperature—we introduced a cold temperature scaling function in CARDAMOM to regulate photosynthetic productivity. We found that GPP was gradually inhibited at **temperature** below 6.0 °C (± 2.6 °C) and completely inhibited below -7.1 °C (± 1.1 °C). The addition of this scaling factor improved the model's ability to replicate spring GPP at interannual and decadal time scales ($r = 0.88$), relative to the nominal CARDAMOM configuration ($r = 0.47$), and improved spring GPP model predictability outside of the data assimilation training period ($r = 0.88$). While cold temperature limitation has an important influence on spring GPP, it does not have a significant impact on integrated growing season GPP, revealing that other environmental controls, such as [precipitation](#), play a more important role in annual productivity.

41 This study highlights growing season onset temperature as a key limiting factor for spring growth in [winter-dormant](#)
42 evergreen forests, which is critical in understanding future responses to climate change.

43 1. Introduction

44 Northern hemisphere evergreen forests contribute significantly to terrestrial carbon (C) storage and exchange
45 (Beer et al., 2010; Thurner et al., 2014). High-[latitude and high-elevation](#) evergreen forests show increasing gross
46 primary productivity (GPP) with increasing temperature driven in large part by earlier growing seasons (Myneni et
47 al., 1997; Randerson et al., 1999; Forkel et al., 2016; Winchell et al., 2016; Lin et al., 2017). However, the response
48 of gross and net C fluxes to warming remains uncertain, especially in subalpine temperate forests, which can
49 experience freezing temperature while still absorbing large amounts of sunlight; both these factors ultimately
50 influence the timing and magnitude of GPP (Bowling et al., 2018). In particular, warmer springs can also lead to
51 earlier snowmelt, which can reduce spring C uptake through increased surface exposure to colder ablation-period air
52 temperatures (Winchell et al., 2016), and can reduce summer C uptake via drought (Hu [et al., 2010](#)). Many
53 subalpine forests in western North America are also highly water limited, with warming and earlier snow melt
54 creating accumulated water deficits, increased drought stress, and growing season C uptake losses (Wolf et al.,
55 2016; Sippel et al., 2017; Buermann et al., 2018, Goulden and Bales, 2019); these factors ultimately make subalpine
56 forest ecosystems sensitive to the direct and indirect effects of climate change and other disturbances, including the
57 effects of droughts, fires and insect infestations ([Keenan et al., 2014](#); [Frank et al., 2014](#); Knowles et al., 2015). The
58 uncertainty in the temperature sensitivity of springtime GPP, increasing vulnerability to [disturbance](#), and GPP
59 modeling challenges (Anav et al., 2015) create urgency to improve our ability to observe and model these
60 ecosystems to understand how C exchange will be altered in a warming climate.

61 Fortunately, availability of long term ecosystem observations is improving. The expansion of international
62 flux tower networks over the last three decades (e.g. AmeriFlux, FLUXNET, ChinaFLUX, ICOS) has greatly
63 improved C flux sampling across global ecosystems at 1 km scale ([Baldocchi 2008](#); [Baldocchi et al., 2018](#)), and the
64 number of spaceborne sensors continues to grow, allowing global estimation of gross primary production (GPP) and
65 net ecosystem C exchange (NEE) over the last decade (e.g. Stavros et al., 2017; Sun et al., 2017; Schimel et al.,
66 2019). While uncertainties in estimating C fluxes from in situ and satellite data [remain](#) a challenge, the expanding
67 observational record offers a great opportunity to study the temperature sensitivity of subalpine forests at multiple
68 temporal scales.

69 The range of modeling tools available to quantify and study major C pools under ever growing
70 observational constraints is also increasing. Process-based models, in general terms, use explicit mathematical
71 relationships to mechanistically describe bio-physical processes (Korzukhin et al., [2011](#); [Huxman et al., 2003](#);
72 Keenan et al., 2012). In contrast, model-data fusion (MDF) is a relatively new tool that alters model parameters [to](#)
73 [statistically reduce mismatches between observations and model predictions](#) (Raupach et al., 2005; Wang et al.,
74 2009; Keenan et al., 2012). MDF methods can be used to statistically represent the terrestrial C balance by
75 generating optimized state and process variable parameterizations, with uncertainties, which best match the signal
76 and noise in observations (Bloom et al., 2020).

Deleted: 1996

78 Models of varying complexity and assimilation capabilities have been used to study how C exchange varies
79 with temperature in subalpine evergreen ecosystems (e.g., Moore et al., 2008; Scott-Denton et al., 2013; Knowles et
80 al., 2018). Moore et al. (2008) used a simplified ecosystem function model and assimilated C flux data from the
81 Niwot Ridge (US-NR1) subalpine evergreen forest [AmeriFlux](#) tower in Colorado to show the importance of accurate
82 meteorological forcing for parameter optimization and the usefulness of assimilating C flux data for determining
83 connections between the C and water cycles. Scott-Denton et al. (2013) integrated meteorological and flux data
84 from 1999-2008 from the same site with an ensemble of more sophisticated Earth System Models (ESM) and
85 showed higher rates of C uptake by the end of the 21st century associated with warming and lengthening growing
86 seasons, and driven by greater increases of spring GPP relative to late season respiration.

87 Interestingly, model and empirical studies of the C flux response to climate at US-NR1 focus on the 2000-
88 2011 period, which saw increasing summer drought coupled with sustained declines in spring temperature and GPP.
89 US-NR1 has since experienced a gradual recovery of spring GPP with increased spring warming throughout 2011-
90 2018 (Fig. 1), which begs the question: what is the temperature sensitivity of spring GPP over multiple decades of
91 spring cooling and warming at US-NR1, and how well can data-constrained models reproduce long term variability?
92 To answer this question, we combine a mechanistic ecosystem C model (Data Assimilation Linked Ecosystem
93 Carbon, *or* DALEC2; Williams et al., 2005; Bloom et al., 2016) with the CARbon DATA-MODEL fraMework
94 (CARDAMOM; Bloom and Williams, 2015; Bloom et al., 2020) driven by observed meteorological forcing and
95 constrained against eddy covariance fluxes at US-NR1, to investigate the temperature sensitivity of this subalpine
96 evergreen forest at seasonal and interannual timescales. We introduce a new cold temperature limitation function,
97 trained on observed temperature, for more realistic simulation of spring GPP onset. The use of high quality and long
98 term (2000-2018) meteorology and partitioned GPP data at US-NR1 to drive and constrain the model enables robust
99 statistical analysis of interannual variability (IAV), and assessment of “model predictability” through training and
100 validation against subsets of data. We also leverage a recent model intercomparison study (Parazoo et al., 2020),
101 driven by site level meteorological data at US-NR1, to provide a model benchmark assessment, and extract any
102 common environmental controls on modeled GPP. Finally, we examine whether using a decade of flux tower-
103 derived GPP observations to train the model is sufficient to match and predict seasonal to annual patterns in GPP.
104 Given the complexity of carbon-water cycle interactions during the growing (summer) season in this highly water
105 limited ecosystem, and the relatively weak correlation between tower-derived spring and summer GPP ($r = -0.31$, p
106 $= 0.20$), we focus on spring GPP-temperature interactions, with the aim to resolve just one piece of the larger,
107 complex problem of understanding changes in C uptake in a subalpine evergreen ecosystem.

108 2. Materials & Methods

109 2.1. Study Site: Niwot Ridge, CO., USA

110 Our study focuses on an AmeriFlux (<https://ameriflux.lbl.gov/>) core site in Niwot Ridge, Colorado, USA
111 (US-NR1, 40°1'58''N; 105°32'47'' W), where a tower-based eddy covariance system has been used to continuously
112 monitor the net ecosystem exchange (NEE) of carbon dioxide over a subalpine forest since November 1998. The 26

Deleted: ure

Deleted: da

Deleted: l

Deleted: are

Deleted: sufficiently robust

Deleted: measuring

119 m tall tower is located in a high elevation (3050 m) subalpine site in the Rocky Mountains of Colorado (Monson et
120 al., 2002). Located in an evergreen needleleaf (ENF) ecosystem, the dominant tree species include lodgepole pine
121 (*Pinus contorta*), subalpine fir (*Abies lasiocarpa*), and Engelmann spruce (*Picea engelmannii*) (Turnipseed et al.,
122 2002; Turnipseed et al., 2004). Average annual precipitation is 800 mm, with a majority of precipitation falling in
123 the winter as snow (Greenland, 1989; Knowles et al., 2015), which creates a persistent winter snowpack from
124 November through early June (Bowling et al., 2018).

125 2.2. Observations

126 NEE measurements are screened for calm conditions using the standard u_{star} filtering, gap-filled, and
127 partitioned into GPP and ecosystem respiration based on the relationship between nighttime NEE
128 (photosynthetically active radiation, PAR < 50 $\mu\text{mol m}^{-2} \text{s}^{-1}$) and air temperature (Reichstein et al., 2005; Wutzler et
129 al., 2018). Monthly averages of GPP based on nighttime partitioning show similar seasonal structure to results found
130 using an alternative daytime partitioning algorithm (Lasslop et al., 2009), so only nighttime partitioned GPP data are
131 reported here. All GPP estimates are processed as half hourly means, then averaged monthly. Details on the flux
132 measurements, data processing and quality control are provided in Burns et al. (2015).

Deleted: 10

133 2.3. The CARDAMOM Model-Data Fusion System

134 The CARbon DAta-MOdel FraMework (CARDAMOM; Bloom et al., 2016; Yin et al., 2020; Exbrayat et
135 al., 2018; Smallman et al., 2017; Quetin et al., 2020; López-Blanco et al., 2019; Famiglietti et al., 2021; Bloom et
136 al., 2020; amongst others) uses carbon cycle and meteorological observations to constrain carbon fluxes, states and
137 process controls represented in the DALEC2 model of terrestrial C cycling (Williams et al., 2005; Bloom and
138 Williams, 2015). Specifically, CARDAMOM uses a Bayesian model-data fusion approach to optimize DALEC2
139 time-invariant parameters (such as leaf traits, allocation and turnover times) and the “initial” C and H₂O conditions
140 (namely biomass, soil and water states at the start of the model simulation period).

Deleted: o

Deleted: 7

Deleted: 0

141 The DALEC model (Williams et al., 2005; Rowland et al., 2014; Fox et al., 2009; Richardson et al., 2010;
142 Famiglietti et al., 2021; Bloom & Williams, 2015; amongst others) is a box model of C pools connected via fluxes
143 that has been used to evaluate terrestrial carbon cycle dynamics across a range of ecosystems and spatial scales. In
144 all site, regional, and global applications, DALEC parameters are subject to very broad, but physically realistic, prior
145 distributions, and independently estimated and constrained by available observations at each grid point. Here we use
146 DALEC version 2 (DALEC2; Yin et al., 2020; Quetin et al., 2020; Bloom et al., 2020); gross and net carbon fluxes
147 are determined as a function of 33 parameters, including 26 time-invariant parameters relating to allocation, turnover
148 times, plant traits, respiration climate sensitivities, water-use efficiency and GPP sensitivity to soil moisture, and 7
149 parameters describing the initial conditions of live biomass pools (live biomass C, dead organic C and plant-
150 available H₂O). Within DALEC2, GPP estimates are generated in the aggregated canopy model (ACM, Williams et
151 al., 1997); the ACM is derived from simple functional relationships with environmental and plant structural and
152 biochemical information (Williams et al., 1997), that are produced from a sensitivity analysis of GPP estimates from

Deleted: 0

Deleted: which comprise

Deleted: of

Deleted: e

161 the more comprehensive SPA land surface model scheme (Williams et al., 1996, Williams et al., 2001). ACM GPP
 162 estimates are contingent on plant structural and biochemical variables (including LAI, foliar nitrogen and nitrogen-
 163 use efficiency) and meteorological forcing (total daily irradiance, maximum and minimum daily air temperature, day
 164 length, atmospheric CO₂ concentration). In DALEC2, water limitation on ACM is prescribed as a linear response to
 165 soil water deficit (Bloom et al., 2020). For more details on the model-data fusion methodology and CARDAMOM
 166 ensembles, we refer the reader to Appendix A. For a comprehensive overview of the DALEC2 model, we refer the
 167 reader to Bloom et al. (2020) and references therein.

Deleted: s

Deleted: .

168 2.4. Experiment Design

169 In order to develop model experiments that could reliably evaluate temperature-GPP interactions, we first
 170 examine the observed environmental controls on tower-derived GPP. We focus on GPP during spring, defined here
 171 as the period from March-May, which encompasses the climatological onset of GPP and transition from dormant
 172 winter conditions to peak summer conditions (Fig. 1a). Mean spring GPP exhibits large interannual variability (IAV)
 173 with both a small decreasing trend from 2000-2010 (-0.02 g C m⁻² day⁻¹ per year) and increasing trend from 2010-
 174 2018 (0.04 g C m⁻² day⁻¹ per year) (Fig. 1b). Comparison to tower observed temperature data (Fig. 1b and Fig. 2)
 175 shows that spring GPP is positively correlated to mean spring air temperature (Pearson's linear $r = 0.89$, $p =$
 176 0.000004) and summer (June-September) air temperature ($r = 0.10$, $p = 0.70$, Fig. S1a). Mean winter (December-
 177 February) precipitation also has a positive correlation with spring GPP, ($r = 0.07$, $p = 0.77$, Fig. S1b), but it is much
 178 smaller than spring temperature. At interannual timescales, mean annual GPP shows a small increasing trend
 179 (0.0072 g C m⁻² day⁻¹ per year) over the time period (Fig. S2), and largest correlation with winter (December –
 180 February) precipitation (Pearson's linear $r = 0.63$, $p = 0.003$, Fig. S3d) and shortwave irradiance ($r = -0.30$, $p = 0.22$,
 181 Fig. S3f). In contrast, spring temperature shows little correlation with mean annual GPP ($r = -0.02$, $p = 0.92$, Fig.
 182 S3c). It appears that winter precipitation and total irradiance are the dominant drivers in annual productivity, both of
 183 which are correlated, while spring temperature show a first order effect in driving spring GPP.

Deleted: in the traditional sense

Deleted: A

Deleted: B

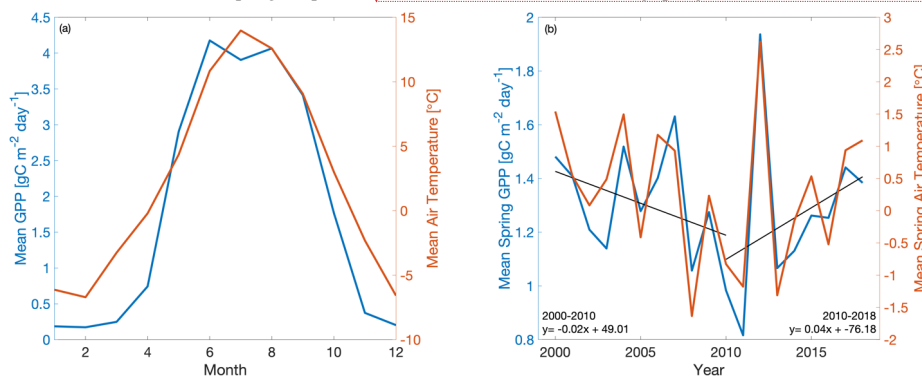
Deleted: A

Deleted: 1

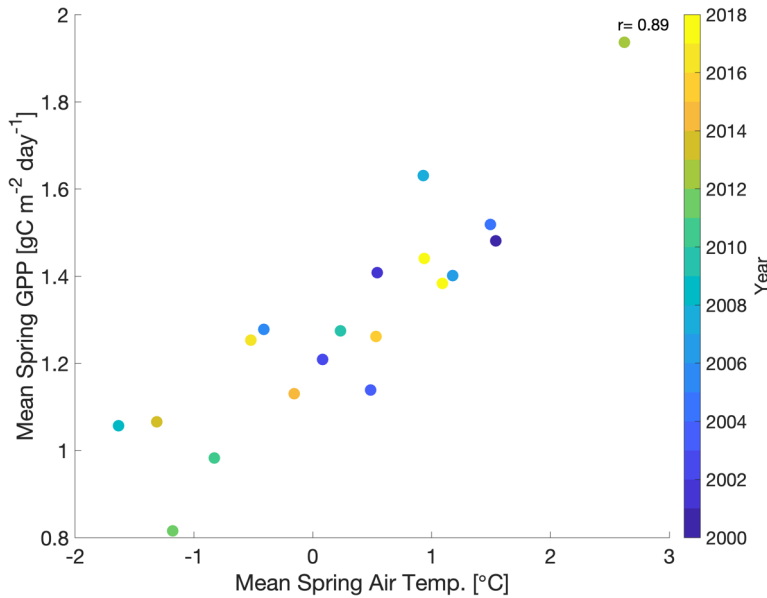
Deleted: 2

Deleted: 3

Deleted: s



184
 185 **Figure 1. Time series of (a) mean monthly GPP (blue) and air temperature (orange) and (b) mean spring (March-May) GPP and**
 186 **air temperature at Niwot Ridge (US-NR1) from 2000-2018. GPP data are derived using a nighttime partitioning technique based**
 187 **on tower observations of NEE and air temperature.**



199

200

201

202

Figure 2. Scatterplot of mean spring (March-May) GPP with mean spring air temperature with the color bar showing the corresponding year (2000-2018). 'r' is Pearson's correlation coefficient.

203

204

205

206

207

208

209

210

211

212

213

214

215

216

We also find that cold temperature has an important limitation on seasonal GPP at US-NR1. The seasonal cycle of GPP shows peak productivity in early summer (around June) and falling to near-zero values by early winter (November), continuing through late winter (February-March). Comparison of monthly GPP and minimum, maximum, and mean monthly air temperature shows an initiation of photosynthesis at monthly maximum air temperature above 0 °C (Fig. 3a) and monthly minimum air temperature above -5 °C (Fig. 3b). The strong dependence of monthly GPP on temperature is consistent with previous findings that temperature is an important driver of spring onset and seasonal variability of GPP in evergreen forests (e.g., Pierrat et al., 2021; Parazoo et al., 2018; Euskirchen et al., 2014; Armeth et al., 2006). As temperature falls in winter dormant plants, productivity becomes negligible. Productivity is triggered again when spring air temperature becomes warm enough to thaw stems, trigger xylem flow and promote access to soil moisture (e.g., Pierrat et al., 2021; Bowling et al., 2018; Ishida et al., 2001). Due to this observed dependence of GPP on temperature at US-NR1, we focus our analysis specifically on spring GPP, where we hypothesize that cold temperature is the dominant control on spring GPP variability.

Deleted: ~

Deleted: maximum

Deleted: in

Deleted: when sufficient radiation is available for absorption by green needles, and

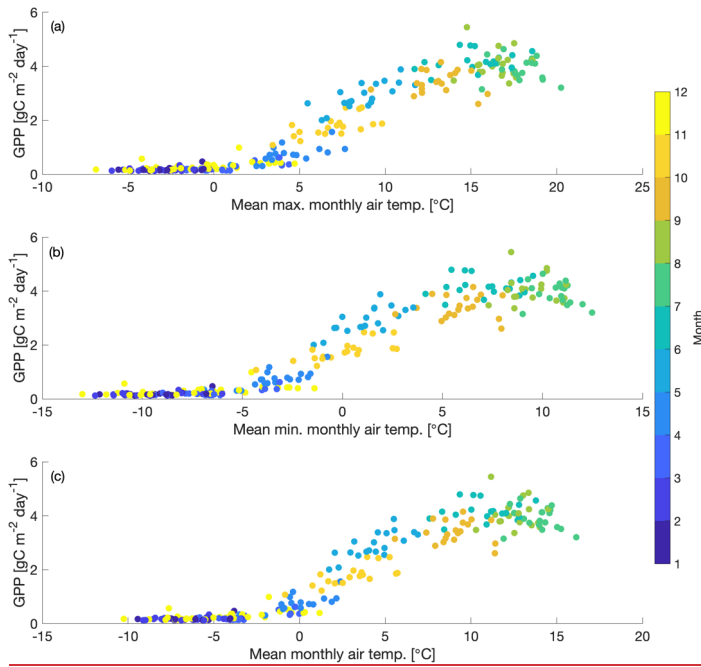


Figure 3. Scatter plot of mean monthly GPP vs. a.) mean maximum air temperature, b.) mean minimum air temperature and c.) mean air temperature for 2000-2018. Dots are colored with the corresponding month.

Deleted: average

In the baseline version of CARDAMOM, seasonal GPP in DALEC2 is limited primarily by incoming shortwave radiation. This light-focused limitation works well for deciduous forests where spring temperature and sunlight are correlated, as well as high latitude regions where sunlight is limited. However, for reasons discussed above, this method fails in evergreen forests such as Niwot Ridge whose green canopies are exposed to high sunlight and below-freezing temperature in spring. As such, we implement a cold temperature scaling factor (g) in DALEC2 Eq.(1), to act as a thermostat that regulates evergreen needleleaf carbon uptake phenology. This scaling factor is developed by analyzing the relationship between monthly minimum & maximum air temperature with tower-derived monthly GPP, where

$$\text{If: } T_{min}(t) < T_0 : g = 0 \quad (1)$$

$$\text{If: } T_{min}(t) > T_g : g = 1$$

$$\text{Else: } g(t) = \frac{(T_{min}(t) - T_0)}{(T_g - T_0)}$$

$$\text{GPP}_{cold}(t) = \text{GPP}(t) * g(t) \quad (2)$$

$T_{min}(t)$ is the observed minimum temperature at Niwot Ridge at time t , $\text{GPP}(t)$ is the nominal ACM-based DALEC2 GPP estimate (see section 2.3) and GPP_{cold} is the corresponding cold temperature GPP estimate. Equation (2) may represent changes in plant hydraulics and photosynthetic activity due to changing temperature in the spring. As

Deleted: where

Formatted: Font: Not Italic

243 temperature increases, evergreen stems slowly thaw, which enables the trees to access available soil moisture and
 244 slowly reactivate their carbon and water exchange processes (Mayr et al., 2014; Bowling et al., 2018). Temperature
 245 also impacts the reactivation of photosynthetic activity after winter dormancy (Öquist and Huner, 2003; Tanja et al.,
 246 2003). For example, fluctuating temperature in the spring has been shown to limit and sometimes reverse the
 247 activation of biochemical processes needed for photosynthesis recovery (Ensminger et al., 2004). Exposure to cold
 248 temperature, when combined with increased irradiance in the spring, can also damage evergreen trees (Öquist and
 249 Huner, 2003; Yang et al., 2020), therefore disrupting CO₂ assimilation. These processes may be approximated by
 250 this cold temperature scaling factor added to CARDAMOM. The temperature thresholds for photosynthesis
 251 shutdown (referred to as T₀) and initiation (referred to as T_g) are added as model parameters in DALEC2, bringing
 252 the total number of parameters to 35. These 35 DALEC parameters are simultaneously optimized in CARDAMOM.
 253 The CARDAMOM Bayesian-inference probability distributions (see Appendix A) for the T₀ (-7.1 ± 1.1 °C) and T_g
 254 (6.0 ± 2.6 °C) parameters used to define the cold temperature limitation are plotted in Fig S4. We refer to the cold
 255 temperature constrained version of DALEC2 (within CARDAMOM) as DALEC2cold.
 256 The baseline (DALEC2) and cold temperature (DALEC2cold) versions of the model are run for the 2000-
 257 2018 period using tower observed, gap-filled, monthly meteorological (MET) drivers (including minimum and
 258 maximum air temperature, shortwave radiation, vapor pressure deficit, and precipitation). We conduct four
 259 experiments, summarized in Table 1: experiments using DALEC2 and DALEC2cold within CARDAMOM, where
 260 19 years of GPP data are assimilated (referred to as CARD and CARDcold), and a corresponding pair of
 261 experiments where only the first decade of data (2000-2009) is assimilated (referred to as CARD-Half and
 262 CARDcold-Half) and the second decade of data (2010-2019) is withheld for validation, as a train-test scenario. All
 263 months of GPP data are assimilated into the model, however our analysis focuses on the constraints on spring
 264 (March-May) GPP. These four experiments serve to evaluate the sensitivity of modeled GPP at Niwot Ridge to cold
 265 temperature limitation and parameter optimization. Specifically, the objective of experiments “CARD” and
 266 “CARDcold” is to determine whether the cold temperature scaling factor improves the representation of spring GPP
 267 variability across the 2000-2018 period; the objective of experiments “CARD-Half” and “CARDcold-Half” is to
 268 cross-validate the predictive skill of CARDcold by assessing whether the addition of a cold temperature scaling
 269 factor, informed by a subset of GPP data, can improve prediction of a withheld subset of GPP data.

- Formatted: Font: Not Italic
- Formatted: Font: Not Italic
- Formatted: Font: Not Italic
- Formatted: Font: Not Italic
- Formatted: Font: Not Italic
- Formatted: Font: Not Italic
- Formatted: Font: Not Italic, Subscript
- Formatted: Font: Not Italic
- Formatted: Font: Not Italic
- Formatted: Font: Not Italic
- Deleted: 3

- Deleted: 1
- Deleted: ,
- Deleted: , and data assimilation

270
271
272
273
274
275
276
277
278
279

284
285

Table 1. Summary of CARDAMOM modeling experiments to determine sensitivity of seasonal and interannual spring GPP variability to cold temperature limitation (CARD vs CARDCold) and the ability to perform outside training window (Half).

Experiment Name	Met. Drivers	Time Period	GPP assimilation	Time period considered in assimilation	Uncertainties in GPP	Cold Temp. Limitation
CARD	yes	2000-2018	yes	2000-2018	20%	No
CARD-Half	yes	2000-2018	yes	2000-2009	20%	No
CARDCold	yes	2000-2018	yes	2000-2018	20%	Yes
CARDCold-Half	yes	2000-2018	yes	2000-2009	20%	Yes

286

287 2.5. Comparison to Terrestrial Biosphere Model Ensemble

288 A recent model intercomparison study provides an ideal benchmark for evaluating CARDAMOM
 289 simulations (section 2.4). Parazoo et al. (2020) conducted an experiment in which an ensemble of state-of-the-art
 290 terrestrial biosphere models (TBMs) were forced by the same observed meteorology at Niwot Ridge from 2000-2018,
 291 but with differences in spin-up, land surface characteristics, and parameter tuning. The TBMs are designed to simulate
 292 the exchanges of carbon, water, and energy between the biosphere and atmosphere, from global to local scales
 293 depending on inputs from meteorological forcing, soil texture, and plant functional type (PFT). The experiment was
 294 designed primarily to evaluate simulations of solar induced fluorescence (SIF) and GPP, the latter of which we focus
 295 on here. We refer the reader to Parazoo et al. (2020) for a more complete description of models, within-model
 296 experiments, and between-model differences.

297 The most important model differences worth noting here include the representation of stomatal conductance,
 298 canopy absorption of incoming radiation, and limiting factors for photosynthesis. We analyze a subset of the models
 299 which were run for multiple years, including SiB3 and SiB4 (Simple Biosphere model versions 3 and 4, respectively),
 300 ORCHIDEE (Organizing Carbon and Hydrology in Dynamic Ecosystems), BEPS (Boreal Ecosystems Productivity
 301 Simulator), and CLM4.5 and CLM5.0 (Community Land Model Versions 4.5 and 5.0, respectively). We also analyze
 302 within-model experiments in SiB3 and ORCHIDEE to isolate effects related to prescription of leaf area index (LAI;
 303 monthly varying in SiB3-exp1, fixed at 4.0 m²/m² in SiB3-exp2), temperature and water stress (ORCHIDEE-exp1
 304 includes temperature stress; ORCHIDEE-exp2 accounts for temperature and water stress), and data assimilation
 305 (ORCHIDEE-exp3, in which a subset of model parameters controlling photosynthesis and phenology are optimized
 306 against global OCO-2 SIF data, Bacour et al., 2019). Most of the TBM model experiments were run with default
 307 parameters (BEPS, CLM50, SiB3, SiB4, ORCHIDEE-exp1 and exp2). The other experiments were optimized in the
 308 following ways: either a) parameters were hand-tuned based on the US-NR1 data (CLM45) or b) the parameters were

Deleted: -

Deleted: Ecosystems

Formatted: Font: Not Italic

311 [optimized using OCO-2 SIF data \(ORCHIDEE-exp3\)](#). For more details on the parameterization of the TBM-SIF
 312 [experiments, we refer the reader to Parazoo et al. \(2020\)](#). The use of these models provides insight into the spread in
 313 [model structures and the use of their default parameters](#). Finally, we note that not all model simulations span the entire
 314 observed record (2000-2018). While our analysis focuses on the [long-term](#) record from 2000-2018, we provide
 315 multiple comparisons to ensure consistency of time period: (1) IAV from 2001-2018 for SiB3, SiB4, ORCHIDEE,
 316 and CLM4.5; (2) IAV from 2012-2018 for SiB3, SiB4, ORCHIDEE, CLM4.5, and CLM5.0, [and](#) (3) ~~seasonal~~
 317 variability from 2015-2018 for all models. We refer to the ensemble of models and within model experiments
 318 collectively as TBM-MIP.

Deleted: long term

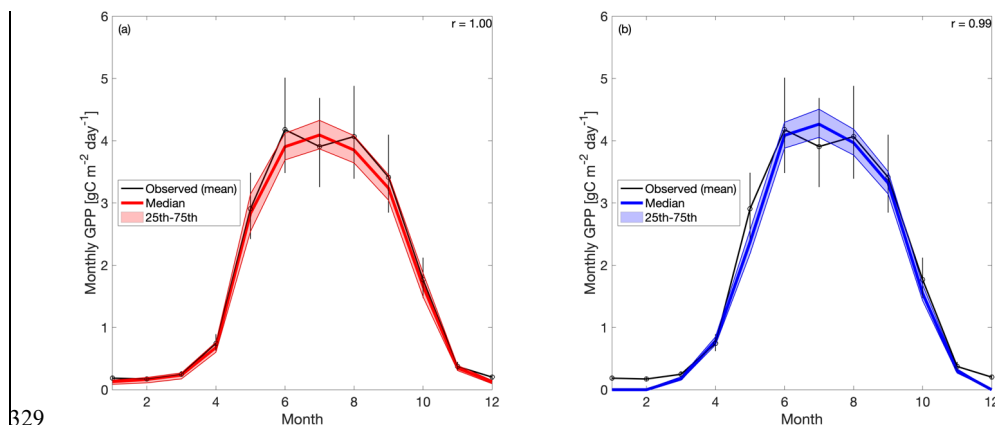
Deleted: S

319 3. Results & Discussion

320 3.1. Evaluation of CARDAMOM 2000–2018 GPP

321 When the 19 years of tower-derived GPP data are assimilated into both versions of the model, the mean
 322 seasonal cycle is accurately replicated (Fig. 4). The Pearson's r values for CARD (Fig. 4a) and CARDcold (Fig. 4b)
 323 are almost equal ($r = 1.00$ and 0.99) with minimal increases in root mean square error (RMSE) and mean bias error
 324 (MBE) for CARDcold (RMSE = $0.24 \text{ g C m}^{-2} \text{ day}^{-1}$ and $0.23 \text{ g C m}^{-2} \text{ day}^{-1}$, MBE = $0.06 \text{ g C m}^{-2} \text{ day}^{-1}$ and 0.19 g C
 325 $\text{m}^{-2} \text{ day}^{-1}$ for CARD and CARDcold, respectively). Assimilating only the first decade of GPP data (Half
 326 experiments) does not drastically alter model performance (Fig. S5), with only slight changes in RMSE and MBE
 327 ($\Delta\text{RMSE} = 0.008 \text{ g C m}^{-2} \text{ day}^{-1}$, $\Delta\text{MBE} = 0.03 \text{ g C m}^{-2} \text{ day}^{-1}$ for CARD-Half, $\Delta\text{RMSE} = -0.003 \text{ g C m}^{-2} \text{ day}^{-1}$,
 328 $\Delta\text{MBE} = 0.02 \text{ g C m}^{-2} \text{ day}^{-1}$ for CARDcold-Half).

Deleted: 4



329 **Figure 4.** Tower-derived [average monthly GPP](#) (black line) and modeled GPP seasonal cycles at US-NR1 for 2000-2018, for a.)
 330 CARD and b.) CARDcold experiments. The half-assimilation experiments (CARD-Half and CARDcold-Half) can be found in
 331 the supplement (Fig S5). Model outputs include the median value of each experiment (bold color line) with the 25th-75th
 332 percentiles of the ensembles (shaded area). The median is plotted instead of the mean to avoid impact of outlier ensemble
 333 members ($N = 4000$). Error bars = tower-derived GPP multiplied/divided by $\exp(\sqrt{\log(2)/2^2n}/n)$, $n = \#$ of years in average (n
 334 $= 19$). 'r' is the Pearson's coefficient.

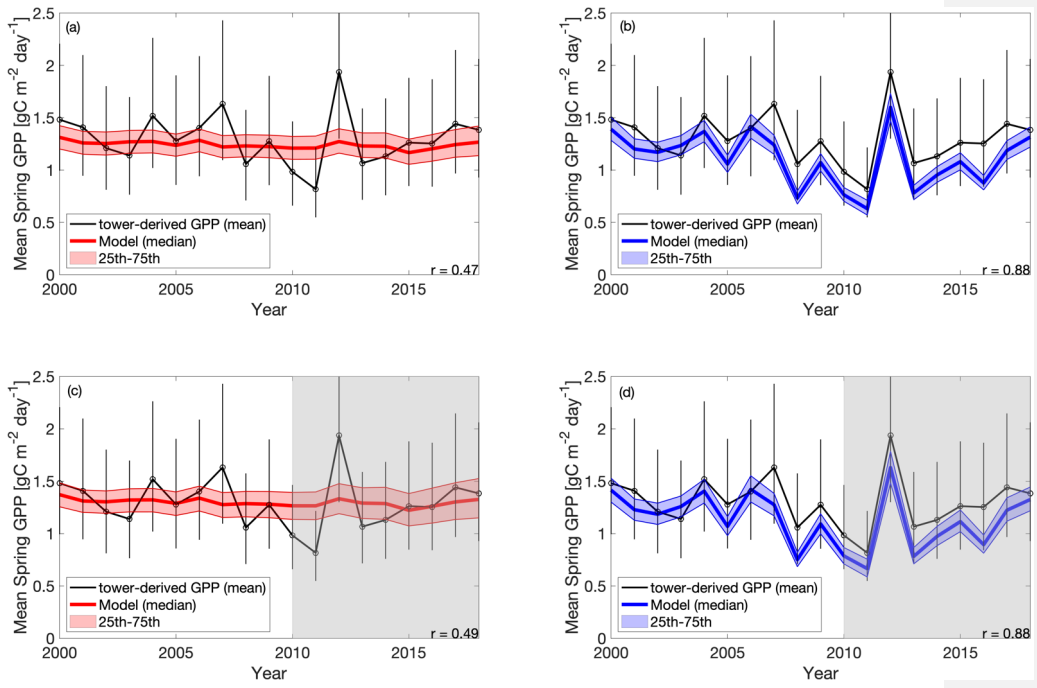
Deleted: , averaged

Deleted: 4

341
342
343
344
345
346
347
348
349
350
351
352
353
354
355
356
357

The cold experiments exhibit an improved fit to the observed IAV in spring productivity (Fig. 5), relative to CARD, ($r = 0.47$, $\text{std} = 0.03 \text{ g C m}^{-2} \text{ day}^{-1}$ for CARD; $r = 0.88$, $\text{std} = 0.27 \text{ g C m}^{-2} \text{ day}^{-1}$ for CARDcold). CARDcold also has slightly reduced RMSE ($-0.01 \text{ g C m}^{-2} \text{ day}^{-1}$) and larger MBE ($0.13 \text{ g C m}^{-2} \text{ day}^{-1}$). Similar to the seasonal cycle analysis, the assimilation of only the first decade of GPP data (Half experiments) has minimal impact on model performance ($\Delta\text{RMSE} = 0.007 \text{ g C m}^{-2} \text{ day}^{-1}$, $\Delta\text{MBE} = 0.06 \text{ g C m}^{-2} \text{ day}^{-1}$ for CARD-Half, and $\Delta\text{RMSE} = 0.02 \text{ g C m}^{-2} \text{ day}^{-1}$, $\Delta\text{MBE} = 0.02 \text{ g C m}^{-2} \text{ day}^{-1}$ for CARDcold-Half). We find less agreement between modeled and tower-derived GPP IAV in summer for both CARD and CARDcold (CARD $r = 0.32$, $\text{std} = 0.11 \text{ g C m}^{-2} \text{ day}^{-1}$; CARDcold $r = 0.05$, $\text{std} = 0.10 \text{ g C m}^{-2} \text{ day}^{-1}$; Fig. S6). While there is little variation in RMSE between the half and full-assimilation experiments, RMSE is larger for summer than spring GPP (average RMSE = $0.23 \text{ g C m}^{-2} \text{ day}^{-1}$ for spring model outputs, average RMSE = $0.35 \text{ g C m}^{-2} \text{ day}^{-1}$ for summer model outputs). Model agreement is further reduced when considering annual average GPP (Fig. S7, Table S2). Although the cold temperature limitation improves IAV slightly, it is still small compared to observed variability (mean annual $\text{std} = 0.14 \text{ g C m}^{-2} \text{ day}^{-1}$). Correlations to tower-derived GPP at the annual scale are small for both CARD and CARDcold ($r = 0.19$ and $r = 0.22$, Fig. S7a-b). Overall, the cold temperature limitation substantially improves agreement between the model and tower-derived spring GPP, with slight reductions in performance for summer and annual GPP.

Deleted: 1
Deleted: 5
Deleted: 6
Deleted: 6
Deleted: -

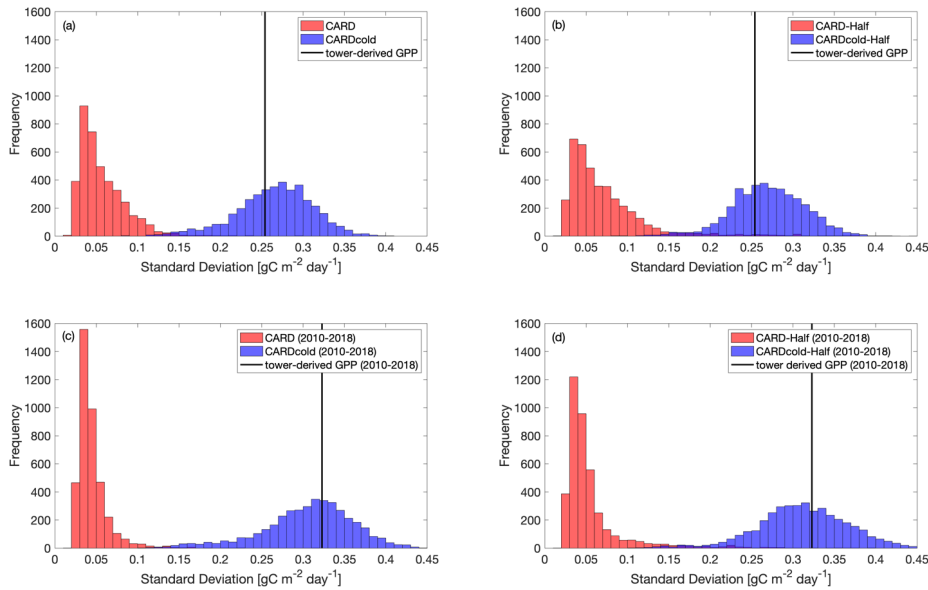


358

364 **Figure 5.** Tower-derived (black line) mean spring (March-May) GPP with model interquartile range (shaded area) and median
365 (bold color line) spring GPP outputs for a.) CARD, b.) CARDcold, c.) CARD-Half, and d.) CARDcold-Half experiments. The
366 grey regions indicate no data assimilation (i.e. testing window). Model experiments are the same as in Figure 4. Uncertainty =
367 $\exp(\sqrt{\log(2)^2 \cdot n}/n)$, n=# of months in average (n = 3).
368

369 The standard deviation in tower-derived mean spring GPP (March-May) is approximately $0.25 \text{ g C m}^{-2} \text{ day}^{-1}$.
370 The addition of the cold temperature limitation improves the model's ability to match the IAV of mean spring
371 GPP (Fig. 6a-b). An examination of all modeled scenarios for CARD and CARDcold (i.e. all 4000 DALEC2
372 simulations), shows that the cold temperature limitation produces spring IAV values much closer to what is
373 observed in the tower-derived GPP data. Only 0.3% of CARD ensembles produces mean spring IAV values within
374 20% of the tower-derived spring GPP standard deviation ($0.25 \pm 0.05 \text{ g C m}^{-2} \text{ day}^{-1}$), whereas 69% of CARDcold
375 ensembles have standard deviation values within the same range. Interestingly, assimilating only the first ten years
376 of GPP data (Half experiments, Fig. 6b) slightly increases the number of ensemble members with standard
377 deviations within the mentioned range for both CARD-Half (2.4%) and CARDcold-Half (70%). It is promising to
378 see that despite not assimilating the 2010-2018 GPP data into the model, CARDcold-Half is still able to match
379 average spring IAV of the full data record.

380 We also consider the IAV in spring GPP for just the second half of the data record (2010-2018). IAV of
381 tower-derived spring GPP increases slightly in 2010-2018 ($0.32 \text{ g C m}^{-2} \text{ day}^{-1}$). Once again, the cold temperature
382 limitation enables CARDAMOM to match spring GPP IAV (Fig. 6c-d). 0.03% of CARD ensembles produce mean
383 spring IAV values within 20% of the tower-derived spring GPP standard deviation for the 2010-2018 period ($0.32 \pm$
384 $0.06 \text{ g C m}^{-2} \text{ day}^{-1}$), whereas 76% of CARDcold ensembles have standard deviation values within the same range.
385 For the Half experiments, 0.6% of CARD and 75% of CARDcold ensembles have IAV values within 20% of the
386 standard deviation for 2010-2018. **This improvement in matching IAV is also observed when considering mean**
387 **annual GPP (Fig. S8), but is much smaller than the improvements made for spring GPP.** Overall, CARDcold
388 produces a less biased distribution of IAV values (relative to both assimilated and withheld observations), whereas
389 CARD is more skewed towards smaller IAVs, which indicates that the cold temperature limitation enables a
390 mechanistic and statistical improvement in capturing the interannual variability of spring GPP.
391



392
393
394
395
396
397

Figure 6. Histograms comparing standard deviation in mean spring GPP across all ensembles (N=4000) for CARD (red bars) and CARDcold (blue bars) experiments with a.) full assimilation, b.) half assimilation, c.) full assimilation for the second decade (2010-2018), and d.) half assimilation for the second decade (2010-2018). Black line indicates standard deviation in tower-derived mean spring GPP (std = 0.25 gC m⁻² day⁻¹ for full period (a-b), std = 0.32 gC m⁻² day⁻¹ for 2010-2018 (c-d)).

398 **3.2. Temperature controls on springtime GPP**

399 The added value of the DALEC2 cold temperature limitation for modeling mean spring (March-May) GPP
400 is logically due to large fluctuations in spring temperature at Niwot Ridge. The cold temperature limitation allows
401 DALEC2-CARDAMOM to match the IAV of spring tower-derived GPP closely. Furthermore, the cold temperature
402 limitation enables the model to match tower spring IAV in the second half of the time period (2010-2018) when only
403 the first ten years of GPP data are assimilated (2000-2009). This indicates that the cold temperature limitation is
404 able to estimate spring GPP outside of its training window and could be useful at other sites where data availability
405 is limited. Future work will include evaluating the cold temperature limitation at other sites to ensure that it is
406 applicable beyond Niwot Ridge, for example using forecast skill metrics proposed by Famiglietti et al. (2021).

Deleted: 1

407 Temperature-induced spring onset of GPP is driven by two general processes: (1) initiation of bud burst
408 and leaf expansion leading to increasing LAI, and/or (2) initiation of photosynthetic activity (photosynthetic
409 efficiency i.e., GPP per unit of LAI) due to temperature-induced changes in plant hydraulics (Ishida et al., 2001;
410 Pierrat et al., 2021) or kinetics of the photosynthetic machinery (e.g., Medlyn et al., 2002). In situ LAI
411 measurements suggest that the LAI at Niwot Ridge is relatively constant across the season, which is somewhat
412 expected given the dominant tree species at the site. Hence, the temperature-induced onset of GPP is likely due to

Deleted: 0

415 the latter process, increased photosynthetic efficiency, as supported by the measurements (Figs. 1-2), although small
416 changes in LAI are still feasible given uncertainties in the measurements. The inclusion of the cold temperature
417 limitation scaling factor in the model, a semi-empirical process, leads to a substantial improvement in model
418 representation of GPP at the site. Further development may also look to identify the relative roles of increased LAI
419 and increased photosynthetic efficiency at Niwot Ridge and other evergreen needleleaf sites, as changes in GPP can
420 lead to changes in carbon allocation to LAI, among other plant carbon pools.

421 Temperature is important in both the reactivation of photosynthetic activity in the spring and the wind
422 down of productivity in the fall (Flynn and Wolkovich, 2018; Stinziano and Way, 2017). Therefore, we anticipate
423 that the cold temperature scaling function may also improve our ability to model fall productivity. However, other
424 factors such as water availability and photoperiod must also be considered (Bauerle et al., 2012; Stinziano et al.,
425 2015). Future studies at Niwot Ridge and other sites should investigate the role of these factors (temperature, water,
426 photoperiod) in regulating fall GPP and how we can represent these processes in CARDAMOM.

427 With the inclusion of the cold temperature limitation on GPP and its application in CARDAMOM, we
428 provide a data-constrained estimate of the climate sensitivity of the Niwot Ridge forest to spring temperature.
429 Posterior estimates indicate that GPP is gradually inhibited below $6.0\text{ }^{\circ}\text{C} \pm 2.6\text{ }^{\circ}\text{C}$ (T_g) and completely inhibited
430 below $-7.1\text{ }^{\circ}\text{C} \pm 1.1\text{ }^{\circ}\text{C}$ (T_0). The gradual limitation of GPP by temperature has been observed on hourly and daily
431 timescales in other cold-weather ecosystems, such as Alaskan conifers (Parazoo et al., 2018) and Canadian spruce
432 (Pierrat et al., 2021). This has been connected to the triggering of transpiration and water flow from xylem into
433 leaves (Ishida et al., 2001). However, both biotic (e.g., carotenoid/chlorophyll ratios) and abiotic (e.g., openness of
434 canopy) factors together regulate GPP response to meteorological forcings, and further process-oriented
435 investigations are required to resolve the emergent response of GPP to temperature. For now, this is a useful metric
436 for climate-sensitivity of spring GPP, at least in the absence of long-term adaptations. Furthermore, over the 19 year
437 observation period investigated here the use of a temporally constant T_0 and T_g yields significantly improved GPP
438 estimates, suggesting that much of the variability can be attributed to climate-driven changes, not interannual
439 variation in vegetation parameters. As temperature continues to increase due to climate change (particularly in the
440 early growing season), productivity at US-NR1 could increase as a result and therefore increase carbon uptake, with
441 productivity peaking earlier in the year (e.g., Xu et al., 2016). However, these spring gains in GPP have been shown
442 to not offset the losses of carbon due to summer droughts (e.g., Buermann et al., 2013; Knowles et al., 2018). It is
443 also unclear how the long-term stress of increased temperature could affect forest productivity directly.

444 This study focuses on the relationship between temperature and GPP and its usefulness on model
445 predictions of spring GPP, but an important component that cannot be ignored is the confounding effect of water
446 availability on GPP. Future changes in winter precipitation are more uncertain, therefore limiting our ability to
447 analyze how precipitation changes will alter future productivity. While precipitation observations are analyzed to
448 discern any major connections between GPP and meteorological controls, an analysis of how precipitation affects
449 model predictability is not included in this study. The combined results, including the cold temperature limitation
450 and train-test data assimilation experiments, suggest that other factors besides spring temperature, most notably
451 winter and summer precipitation (Fig. S3) and resulting soil water limitation, also have important impacts on

Deleted: 2

453 summer GPP. We therefore highlight the need to jointly resolve springtime temperature limitation, in conjunction
454 with water stress limitations in future efforts to understand the integrated role of environmental forcings on
455 interannual GPP variability. Furthermore, this analysis does not consider how winter precipitation as snowfall
456 versus rainfall affects productivity, or how resulting changes to winter snowpack could alter productivity long-term.
457 Since annual average GPP appears to be more dependent on winter precipitation/snowpack (Pearson's linear $r =$
458 0.63, Fig. S3a), future work will include improving model predictability of late season productivity and quantifying
459 temperature-water effects on carbon uptake. The definition of the seasons could also alter the connections drawn
460 between seasonal temperature, precipitation and productivity.

Deleted: s

Deleted: ed

461 3.3. Model intercomparison and implications for GPP models

462 Here, we evaluate DALEC2-CARDAMOM against mean spring GPP estimates from TBM-MIP models
463 (Section 2.5 and Parazoo et al. 2020). It is important to remind the reader that the CARDAMOM runs have a
464 significant advantage over the TBM-MIP models in this analysis, as CARDAMOM is trained on US-NR1 GPP data.
465 While TBM-MIP models use tower-observed meteorological inputs, prescribe tower-specific and time-invariant
466 structural properties such as LAI observed at US-NR1 (SiB3-exp2 and CLM4.5), and use data assimilation of global
467 remote sensing data to constrain globally representative plant functional types (ORCHIDEE-exp3), they are not
468 directly constrained by time-varying carbon fluxes at the tower. As such, we emphasize that our model comparison
469 is not a strict assessment of performance, but rather an attempt to learn how model simulation of GPP at an
470 evergreen needleleaf site can be improved.

Deleted: &

Deleted: -

Deleted: competition

Deleted: discern common environmental controls in model performance of simulating the magnitude and seasonal-to-interannual variability of spring GPP at an evergreen needleleaf site...

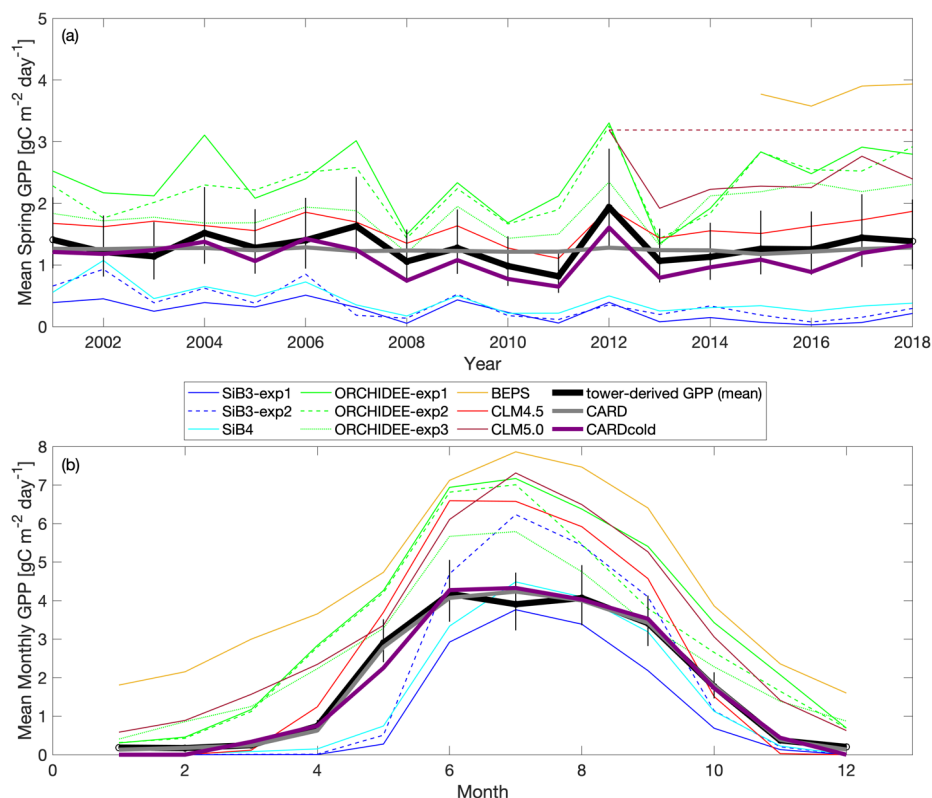
471 There is a wide range in performance of TBM-MIPs in representing the magnitude and IAV of tower-
472 derived spring GPP (Figure 7a). Pearson's r correlations range from 0.25 to 0.82 (mean $r = 0.6$, Table 2) from 2001-
473 2018, with the same models showing slightly improved performance over the second decade (mean $r = 0.73$ from
474 2012-2018). ORCHIDEE-exp1 and CLM4.5 show consistently high performance over all three periods analyzed,
475 with CLM5.0 excelling from 2012-2018, and BEPS from 2015-2018 (Table S1). CLM4.5 also shows the smallest
476 mean bias of the TBM-MIP models (RMSE ~ 0.35), and high agreement in the magnitude of spring GPP variability
477 (1-sigma standard deviation = $0.21 \text{ g C m}^{-2} \text{ day}^{-1}$ for CLM4.5, vs $0.25 \text{ g C m}^{-2} \text{ day}^{-1}$ observed). While
478 acknowledging the advantage of data assimilation, it is promising to see that CARDAMOM (with the addition of the
479 cold temperature limitation) is able to perform comparably to the TBM-MIP models. In particular, CARDcold is
480 well correlated in the direction ($r = 0.88$) and magnitude (1-sigma ~ 0.26) of interannual variability, as well as overall
481 magnitude of spring GPP (low RMSE and MBE).

482 The range of performance across within-model experiments reveals important processes, and uncertainty of
483 process representation, in driving the magnitude and variability of spring GPP. For example, the ORCHIDEE data
484 assimilation experiment (exp3) shows consistently and substantially lower overall correlation (e.g., $r = 0.59$ from
485 2001-2018) than corresponding free running experiments (exp 1 and 2, $r = 0.78-0.82$), but has reduced RMSE and
486 MBE (RMSE = $0.63 \text{ g C m}^{-2} \text{ day}^{-1}$ vs $1-1.14 \text{ g C m}^{-2} \text{ day}^{-1}$). Likewise in SiB3, prescribing an empirically-based but
487 fixed-in-time LAI of $4.0 \text{ m}^2/\text{m}^2$ (exp2) reduces mean bias, but degrades variability ($r = 0.25$) compared to time-
488 variable LAI (exp1) prescribed from satellite data ($r = 0.50$).

Formatted: Superscript

Formatted: Superscript

498
499



500
501
502
503
504
505

Figure 7. Comparison of TBM-MIP models to CARD and CARDcold experiments for a.) mean spring GPP for 2000-2018 and b.) monthly GPP from 2015-2018. Note that fill values are ignored when calculating mean annual values for TBM-MIP experiments. Uncertainty = $\exp(\sqrt{\log(2)^2 \cdot n/n})$, where $n = \#$ years in average ($n = 19$).

Deleted: and b.

506
507
508
509
510
511
512
513

There is also large variability in the modeled seasonal cycle (Fig. 7b) and mean annual GPP (Fig. S9). For mean annual GPP estimates, Pearson's r values are reduced for all models (Table S2). Once again, ORCHIDEE-exp2 and ORCHIDEE-exp3 stand out with some of the higher correlations ($r = 0.60$ and $r = 0.64$) and p -values below 5% significance level. Furthermore, ORCHIDEE-exp3 (temperature stress with SIF data assimilation) has the lowest RMSE and MBE of the model set. SiB3-exp2 (fixed LAI) has a standard deviation closest to "observations" ($0.14 \text{ gC m}^{-2} \text{ day}^{-1}$), and the smallest RMSE and MBE of the TBM models.

Deleted: 7

Most TBM-MIP models capture the shape of the seasonal cycle at Niwot Ridge. For the 2015-2018 period, all models have Pearson's r values larger than 0.91, with p -values much smaller than a 5% significance level (Table

516 S3). With the help of data assimilation, CARDcold accurately captures the seasonal cycle at Niwot Ridge with
 517 reduced error (RMSE = 0.22 g C m⁻² day⁻¹, MBE = 0.07 g C m⁻² day⁻¹), and data assimilation experiments in
 518 ORCHIDEE-exp3 show reduced bias relative to free running experiments. The cold temperature limitation has little
 519 impact on the modeled mean seasonal cycle or mean annual GPP estimates in CARDAMOM, and appears to be
 520 most valuable for improving spring GPP variability.

521
 522 **Table 2.** Pearson's linear r, R-squared, p-value, standard deviation, root mean square error (RMSE), and mean bias error (MBE)
 523 for TBM-MIP and all CARDAMOM experiments to Niwot Ridge tower-derived mean spring (March-May) GPP. Open values
 524 reflect statistics for the 2001-2018 period, while values in parentheses represent the 2012-2018 period. All relevant statistics are
 525 calculated at 5% significance level. *BEPS statistics are not included in this table as this model only has GPP estimates for 2015-
 526 2018.

model	r-value	R-squared	p-value (α = 0.05)	RMSE (gC m ⁻² d ⁻¹)	MBE (gC m ⁻² d ⁻¹)	standard deviation (gC m ⁻² d ⁻¹)
CARD-Half	0.47 (0.55)	0.22 (0.30)	0.05 (0.20)	0.24 (0.26)	-0.005 (0.06)	0.03 (0.04)
CARD	0.45 (0.57)	0.20 (0.33)	0.06 (0.18)	0.24 (0.28)	0.05 (0.12)	0.03 (0.04)
CARDcold-Half	0.88 (0.93)	0.77 (0.86)	0.00 (0.002)	0.21 (0.24)	0.17 (0.22)	0.26 (0.29)
CARDcold	0.87 (0.93)	0.76 (0.87)	0.00 (0.00)	0.23 (0.26)	0.20 (0.24)	0.26 (0.28)
SiB3-exp1	0.50 (0.81)	0.25 (0.66)	0.04 (0.03)	1.07 (1.23)	1.04 (1.21)	0.16 (0.13)
SiB3-exp2	0.25 (0.41)	0.06 (0.17)	0.32 (0.36)	0.97 (1.15)	0.92 (1.13)	0.26 (0.10)
SiB4	0.34 (0.91)	0.12 (0.83)	0.16 (0.00)	0.90 (1.04)	0.86 (1.02)	0.22 (0.09)
ORCHIDEE-exp1	0.82 (0.82)	0.68 (0.67)	0.00 (0.02)	1.14 (1.24)	-1.08 (-1.16)	0.56 (0.67)
ORCHIDEE-exp2	0.78 (0.79)	0.61 (0.63)	0.00 (0.03)	1.00 (1.20)	-0.95 (-1.12)	0.51 (0.64)
ORCHIDEE-exp3	0.59 (0.55)	0.35 (0.31)	0.01 (0.20)	0.63 (0.81)	-0.57 (-0.76)	0.35 (0.36)
BEPS*	X	X	X	X	X	X
CLM4.5	0.82 (0.85)	0.68 (0.73)	0.00 (0.01)	0.34 (0.35)	-0.31 (-0.31)	0.21 (0.18)
CLM5.0	(0.96)	(0.92)	(0.00)	(1.09)	(-1.08)	(0.42)

527
 528 In summary, TBM-MIP experiments reveal several key factors that can improve or degrade estimates of
 529 spring GPP at Niwot Ridge. For example, adapting model parameters to needleleaf species based on hand-tuning to
 530 tower data and formal data assimilation methods (CLM4.5 and ORCHIDEE-exp3, respectively) improves the
 531 overall magnitude of spring GPP. Likewise, prescribing LAI to a constant value of 4.0 m²/m² based on tower
 532 measurements (SiB3-exp2) improves year-to-year variability, while prescribing time variable LAI based on MODIS
 533 data improves spring GPP magnitude (SiB3-exp1). SiB4, which has prognostic rather than prescribed phenology,
 534 represents a compromise in magnitude and variability when looking at the entire record (2001-2018), but is one of
 535 the top performers across all TBM-MIP models over the most recent period (2012-2018).

536 We did not directly consider changes in canopy structural or biophysical characteristics in our
 537 CARDAMOM experiments. In CARDAMOM, LAI is a prognostic quantity (a function of foliar C and leaf carbon
 538 mass per area). In the absence of LAI observational constraints, CARDAMOM LAI is indirectly informed by the
 539 constraints of time-varying GPP on DALEC2 parameters (see section 2.3). Our results suggest that additional
 540 improvements are possible with careful consideration of in situ measured vegetation parameters.

Deleted: 1

Deleted: spring GPP magnitude,

Deleted: year-to-year variability

Deleted: 2

Deleted: 1

Deleted: -

547 TBM-MIP experiments also offer insight on important environmental controls and process representation.
548 Air temperature is an effective constraint of spring GPP onset (CLM4.5, ORCHIDEE-exp1, [Figure 7 and Table 2](#)),
549 but which can be degraded when large scale data assimilation does not account for local- to regional- vegetation
550 characteristics in parameter optimization (e.g., ORCHIDEE-exp3, [Table 2](#)). Water availability appears to be a
551 secondary but still important driver of spring GPP. While acknowledging the numerous differences between
552 CLM4.5 and CLM5.0, we find it important to note that plant hydraulic water stress (CLM5.0) shows improved IAV
553 performance (high correlation, [Table 2](#)) over simplified soil moisture stress functions (CLM4.5). This result further
554 supports efforts to closely analyze seasonal GPP to locate different environmental controls for future model
555 improvements.

556 Our study of the controls of cold temperature on GPP has important implications for modeling seasonal
557 productivity. First, future work must evaluate cold temperature limitation at other sites across an array of ecosystem
558 types. Additionally, it is important to determine if the temperature thresholds of photosynthesis initiation and
559 cessation are similar across locations, or unique to ecosystem type and/or site. Previous studies have had mixed
560 results, supporting both the use of customized temperature threshold parameters dependent on the site (Tanja et al.,
561 2003; Chang et al., 2020) or for a general parameter across multiple sites or biome type (Bergeron et al., 2007).
562 These differences could be due to variations in other variables (e.g., soil temperature, irradiance, etc.) and/or
563 physiological differences in the vegetation species. Identifying how photosynthesis temperature thresholds vary
564 across space and ecosystem type would be beneficial in improving model performance in simulating productivity.
565 Our model intercomparison study also provide insights on how we may improve our ability to model seasonal GPP.
566 For example, in Fig. 7b, we see that the ORCHIDEE model growing season starts too early. In the photosynthesis
567 module of ORCHIDEE, the temperature-dependency of parameters are described by Arrhenius or modified
568 Arrhenius functions following Medlyn et al. (2002) and Kattge and Knorr (2007). In general, the functions are used
569 to estimate the potential rates of Rubisco activity and electron transport based on temperature, as these rates are
570 needed to determine photosynthetic capacity (Medlyn et al., 2002). The lowest temperature for productivity
571 mentioned in these studies are 5°C and 11°C, respectively. Additionally, there is a test at the start of the
572 photosynthesis subroutine that prevents the computation of photosynthesis if the mean temperature over the last 20
573 days falls below -4°C. For our study, the only ORCHIDEE experiment that uses specific data related to the plant
574 functional type of this site (OCO-2 SIF data for US-NR1) is ORCHIDEE-exp3. This experiment improves the
575 general behavior of the modeled GPP seasonal cycle but does not improve ORCHIDEE's ability to capture the start
576 of the growing season. So with the future evaluation of cold temperature limitation at other sites and further study of
577 the potential temperature-influenced bias in the model, then ORCHIDEE (and other process-based models) may
578 need to improve its photosynthesis temperature-dependency for cold plant functional types. Therefore, we
579 recommend implementing a cold temperature GPP limitation in a process-based model to confirm its ability to
580 improve model performance. If we identify (1) how photosynthesis initiation and shutdown varies with temperature
581 and location, and (2) apply a cold temperature limitation successfully in a process-based model, then we could
582 expand our analyses to answer bigger Earth science questions. For example, we could use Earth System Model
583 temperature trends to determine how changing temperature will impact GPP in the future.

Deleted: and reduced error

585 While further experiments are needed, these results demonstrate the value of (1) site-level data assimilation
586 for local scale prediction of GPP magnitude and variability, (2) global data assimilation for reducing magnitude
587 biases, and (3) process formulation for accounting for sensitivity to temperature limitation and water stress. Overall,
588 these results are encouraging for model-data fusion systems which have developed the capacity to bring together
589 temporally and spatially resolved functional and structural vegetation components such as LAI, SIF, soil organic
590 matter, and above- and below-ground biomass (e.g., Bacour et al., 2019; Smith et al., 2020; Bloom et al., 2020).
591 Joint assimilation of these datasets, coupled with observed meteorological forcing, has potential to introduce more
592 emergent constraints of vegetation change with respect to environmental change, thus improving overall estimates of
593 productivity. Future work will assess the joint impact of SIF, ET, LAI, and biomass data as effective constraints on
594 light use and water use efficiency (Smith et al., 2020), which is expected to improve the ability of CARDAMOM to
595 use light with respect to increasing biomass subject to longer growing seasons and heat and water stress.

Deleted: -

596 4. Conclusions

597 Despite mechanistic advances in ecosystem modeling, it is still a challenge to simulate temporal variations
598 in GPP. In an attempt to dissect the environmental controls on GPP in an evergreen needleleaf ecosystem, we
599 analyzed the impact of temperature on spring (March-May) productivity by implementing a cold temperature GPP
600 limitation within a model-data fusion system (DALEC2-CARDAMOM). The cold weather GPP limitation allows
601 for improved model estimates of mean spring productivity at Niwot Ridge, specifically CARDAMOM's ability to
602 match the interannual variability observed in tower-derived mean spring GPP. Furthermore, CARDAMOM is able
603 to match spring interannual variability between model and tower data outside of the training period. When
604 compared to TBM-MIP models, controls that appear to impact model performance include the inclusion of water
605 stress (e.g., soil moisture) and vegetation parameters (e.g., prescription of LAI). The fact that the cold temperature
606 limitation does not improve CARDAMOM's annual GPP estimates suggests that other controls (i.e. winter
607 precipitation) drive GPP variability in other parts of the year, most likely summer (June-September). The cold
608 temperature limitation may prove useful in understanding future changes in spring productivity due to changes in
609 temperature in other ecosystems as well.

Deleted: e.g.

Deleted: important ecosystems, such as the Western U.S

610 Appendices

611 Appendix A: Model-Data Fusion Methodology

612 The DALEC2 model parameter values and state variable initial conditions (henceforth \mathbf{x}) are optimized
613 using a Bayesian inference approach, where the posterior probability distribution of \mathbf{x} given observations \mathbf{O} , $p(\mathbf{x}|\mathbf{O})$,
614 can be expressed as

$$615 p(\mathbf{x}|\mathbf{O}) \propto p(\mathbf{x})L(\mathbf{x}|\mathbf{O}) \quad (\text{A1})$$

616 Where $p(\mathbf{x})$ is the prior probability distribution of \mathbf{x} , and $L(\mathbf{x}|\mathbf{O})$ is the likelihood of the DALEC parameters
617 and initial conditions given observations \mathbf{O} . We define the likelihood function as

$$L(\mathbf{x}|\mathbf{o}) = e^{-\frac{1}{2}\sum_i \left(\frac{m_i(\mathbf{x}) - o_i}{\sigma}\right)^2} + e^{-\frac{1}{2}\sum_a \left(\frac{m'_a(\mathbf{x}) - o'_a}{\sigma'}\right)^2}, \quad (\text{A2})$$

where for monthly timestep i , $m_i(\mathbf{x})$ and o_i represent monthly modeled GPP (based on parameters \mathbf{x}) and flux-tower GPP observation, respectively. Following model-data fusion efforts with a spectrum of temporal modes of variability (Desai 2010, Quetin et al., 2020 and Bloom et al., 2020), we extend the cost function to include mean annual model and tower-derived GPP, $m'_a(\mathbf{x})$ and o'_a respectively) for year = a , which allows the GPP cost function to be sensitive to both seasonal and inter-annual components of the flux tower GPP signal. We log-transform modeled and tower-derived GPP values (as done in Bloom & Williams, 2015 and Bloom et al., 2016), which is preferable for characterize model-data residuals between strictly positive quantities (such as GPP). For lack of better uncertainty estimates on monthly and annual flux tower GPP accuracy—including lack of knowledge on GPP error characteristics at monthly timescales, error covariance between individual GPP estimates, model structural error impacts on GPP—we conservatively prescribed uncertainty factor of $\sigma = 2$ for monthly values (roughly ~75%), and $\sigma' = 1.2$ (~18%) for annual values; in general we found that these values led to robust agreements between flux tower and DALEC2 GPP variability (model-data mismatch metrics are reported in section 3 of the manuscript).

For all model experiments, we sample the probability of $p(\mathbf{x}|\mathbf{o})$, the posterior probability distribution of initial conditions \mathbf{x} given observations \mathbf{o} , we use four Metropolis-Hastings Markov Chain Monte Carlo (MHMCMC; Haario et al. 2001) for 10^8 iterations; we subsample 1000 parameter vectors \mathbf{x} , from the latter 50% of each chain (in total 1000 samples x 4 chains = 4000 samples). We test for convergence in the MHMCMC estimates of \mathbf{x} using a the Gelman-Rubin convergence diagnostic to measure convergence between the four chains.

640 Data Availability

641 The Ameriflux US-NR1 data were obtained from: <https://ameriflux.lbl.gov/sites/siteinfo/US-NR1> (Blanken et al.,
642 2020). The US-NR1 data used in this study, as well as the CARDAMOM and TBM-MIP outputs are publicly
643 available and provided in .nc file format at <http://doi.org/10.5281/zenodo.4928097>.

644 Code Availability

645 The CARDAMOM code used in this study is available here: [https://github.com/CARDAMOM-](https://github.com/CARDAMOM-framework/CARDAMOM_v2.2)
646 [framework/CARDAMOM_v2.2](https://github.com/CARDAMOM-framework/CARDAMOM_v2.2)

647 Author Contributions

648 SGS, NCP and AAB designed and performed the research. AJN, BR, CB, FM, IB, YZ, BQ, and MS contributed
649 model simulations. DRB, SPB, and PDB contributed observational data. All authors contributed to the writing of
650 the paper and/or revision of the manuscript.

Deleted: l

Deleted: l

Deleted: as

654 **Supplement**

655 **Competing Interests**

656 *An author is a member of the editorial board of *Biogeosciences*. The peer-review process was guided by an*
657 *independent editor, and the authors have also no other competing interests to declare.*

658 **Acknowledgements**

659 *The US-NRI AmeriFlux site has been supported by the U.S. DOE, Office of Science through the AmeriFlux*
660 *Management Project (AMP) at Lawrence Berkeley National Laboratory under Award Number 7094866. A portion*
661 *of this research was carried out at the Jet Propulsion Laboratory, California Institute of Technology, under contract*
662 *with NASA. Funding from the NASA Earth Science Division Arctic Boreal Vulnerability Experiment (ABoVE) is*
663 *acknowledged. We acknowledge the MEASUREs program. SGS was partly supported by a University of California,*
664 *Irvine graduate student fellowship. DRB and BMR were supported by the NASA CMS (80NSSC20K0010) and the*
665 *NSF Macrosystems Biology and NEON-Enabled Science (1926090) Programs. The National Center for*
666 *Atmospheric Research (NCAR) is sponsored by NSF. MS was partly supported by the U.S. Department of Energy*
667 *Office of Science Biological and Environmental Research as part of the Terrestrial Ecosystem Science Program*
668 *through the Next-Generation Ecosystem Experiments (NGEE) Tropics project. PNNL is operated by Battelle*
669 *Memorial Institute for the U.S. DOE under contract DE-AC05-76RLO1830.*

670 **References**

671 Anav, A., Friedlingstein, P., Beer, C., Ciais, P., Harper, A., Jones, C., Murray-Tortarolo, G., Papale, D., Parazoo, N.
672 C., Peylin, P., Piao, S., Sitch, S., Viovy, N., Wiltshire, A., and Zhao, M.: Spatiotemporal patterns of terrestrial gross
673 primary production: A review, *Rev. Geophys.*, 53, 785–818, <https://doi.org/10.1002/2015RG000483>, 2015.
674
675 Ameth, A., Lloyd, J., Shibistova, O., Sogachev, A., and Kolle, O.: Spring in the boreal environment: observations on
676 pre- and post-melt energy and CO₂ fluxes in two central Siberian ecosystems, *Boreal Environ. Res.*, 11, 311–328,
677 2006.
678
679 Bacour, C., Maignan, F., MacBean, N., Porcar-Castell, A., Flexas, J., Frankenberg, C., Peylin, P., Chevallier, F.,
680 Vuichard, N., and Bastrikov, V.: Improving Estimates of Gross Primary Productivity by Assimilating Solar-Induced
681 Fluorescence Satellite Retrievals in a Terrestrial Biosphere Model Using a Process-Based SIF Model, *J. Geophys.*
682 *Res. G: Biogeosci.*, 124, 3281–3306, <https://doi.org/10.1029/2019JG005040>, 2019.
683
684 Baldocchi, D. 'Breathing' of the terrestrial biosphere: lessons learned from a global network of carbon dioxide flux
685 measurement systems, *Aust. J. Bot.*, 56, 1–26, <https://doi.org/10.1071/BT07151>, 2008.
686
687 Baldocchi, D., Chu, H., and Reichstein, M.: Inter-annual variability of net and gross ecosystem carbon fluxes: A
688 review, *Agric. For. Meteorol.*, 249, 520–533, <https://doi.org/10.1016/j.agrformet.2017.05.015>, 2018.
689
690 *Bauerle, W. L., Oren, R., Way, D. A., Qian, S. S., Stoy, P. C., Thornton, P. E., Bowden, J. D., Hoffman, F. M., and*
691 *Reynolds, R. F.: Photoperiodic regulation of the seasonal pattern of photosynthetic capacity and the implications for*
692 *carbon cycling. PNAS, 109, 8612–8617, <https://doi.org/10.1073/pnas.1119131109>, 2012.*
693

Deleted: ¶
Formatted: Heading 1
Formatted: Font: Italic
Deleted: The authors declare that they have no conflict of interest.

Deleted: DRB and BMR were supported by the NASA CMS (NNX16AP33G) and the NSF Macrosystems Biology and NEON-Enabled Science (1926090) Programs

Deleted: Agricultural and Forest Meteorology

Deleted: ¶

702 Beer, C., Reichstein, M., Tomelleri, E., Ciais, P., Jung, M., Carvalhais, N., Rödenbeck, C., Arain, M. A., Baldocchi,
703 D., Bonan, G. B., Bondeau, A., Cescatti, A., Lasslop, G., Lindroth, A., Lomas, M., Luysaert, S., Margolis, H.,
704 Oleson, K. W., Rouspard, O., Veenendaal, E., Viovy, N., Williams, C., Woodward, F. I., and Papale, D.: Terrestrial
705 Gross Carbon Dioxide Uptake: Global Distribution and Covariation with Climate, *Science*, 329, 834–838,
706 <https://doi.org/10.1126/science.1184984>, 2010.

707
708 [Bergeron, O., Margolis, H. A., Black, T. A., Coursolle, C., Dunn, A. L., Barr, A. G., and Wofsy, S. C.: Comparison](#)
709 [of carbon dioxide fluxes over three boreal black spruce forests in Canada, *Global Change Biol.*, 13, 89–107,](#)
710 <https://doi.org/10.1111/j.1365-2486.2006.01281.x>, 2007.

711
712 ▼ [Blanken, P.D., Monson, R.K., Burns, S.P., Bowling, D.R., Turnipseed, A.A.: Ameriflux US-NR1 Niwot Ridge](#)
713 [Forest \(LTER NWT1\), Ver. 16-5, AmeriFlux AMP, \(Dataset\). <https://doi.org/10.17190/AMF/1246088>, 2020.](#)

714
715 Bloom, A. A. and Williams, M.: Constraining ecosystem carbon dynamics in a data-limited world: integrating
716 ecological “common sense” in a model–data fusion framework, *Biogeosciences*, 12, 1299–1315,
717 <https://doi.org/10.5194/bg-12-1299-2015>, 2015.

718
719 Bloom, A. A., Exbrayat, J.-F., Velde, I. R. van der, Feng, L., and Williams, M.: The decadal state of the terrestrial
720 carbon cycle: Global retrievals of terrestrial carbon allocation, pools, and residence times, PNAS, 113, 1285–1290,
721 <https://doi.org/10.1073/pnas.1515160113>, 2016.

722
723 [Bloom, A. A., Bowman, K. W., Liu, J., Konings, A. G., Worden, J. R., Parazoo, N. C., Meyer, V., Reager, J. T.,](#)
724 [Worden, H. M., Jiang, Z., Quetin, G. R., Smallman, T. L., Exbrayat, J.-F., Yin, Y., Saatchi, S. S., Williams, M., and](#)
725 [Schimel, D. S.: Lagged effects regulate the inter-annual variability of the tropical carbon balance, *Biogeosciences*,](#)
726 [17, 6393–6422, <https://doi.org/10.5194/bg-17-6393-2020>, 2020.](#)

727
728 ▼ [Bowling, D. R., Logan, B. A., Hufkens, K., Aubrecht, D. M., Richardson, A. D., Burns, S. P., Anderegg, W. R. L.,](#)
729 [Blanken, P. D., and Eiriksson, D. P.: Limitations to winter and spring photosynthesis of a Rocky Mountain](#)
730 [subalpine forest, *Agric. For. Meteorol.*, 252, 241–255, <https://doi.org/10.1016/j.agrformet.2018.01.025>, 2018.](#)

731
732 Buermann, W., Bikash, P. R., Jung, M., Burn, D. H., and Reichstein, M.: Earlier springs decrease peak summer
733 productivity in North American boreal forests, *Environ. Res. Lett.*, 8, 024027, [https://doi.org/10.1088/1748-](https://doi.org/10.1088/1748-9326/8/2/024027)
734 [9326/8/2/024027](https://doi.org/10.1088/1748-9326/8/2/024027), 2013.

735
736 Buermann, W., Forkel, M., O’Sullivan, M., Sitch, S., Friedlingstein, P., Haverd, V., Jain, A. K., Kato, E., Kautz, M.,
737 Lienert, S., Lombardozi, D., Nabel, J. E. M. S., Tian, H., Wiltshire, A. J., Zhu, D., Smith, W. K., and Richardson,
738 A. D.: Widespread seasonal compensation effects of spring warming on northern plant productivity, *Nature*, 562,
739 110–114, <https://doi.org/10.1038/s41586-018-0555-7>, 2018.

740
741 [Burns, S. P., Blanken, P. D., Turnipseed, A. A., Hu, J., and Monson, R. K.: The influence of warm-season](#)
742 [precipitation on the diel cycle of the surface energy balance and carbon dioxide at a Colorado subalpine forest site,](#)
743 [*Biogeosciences*, 12, 7349–7377, <https://doi.org/10.5194/bg-12-7349-2015>, 2015.](#)

744
745 [Chang, Q., Xiao, X., Wu, X., Doughty, R., Jiao, W., Bajgain, R., Qin, Y., and Wang, J.: Estimating site-specific](#)
746 [optimum air temperature and assessing its effect on the photosynthesis of grasslands in mid- to high-latitudes,](#)
747 [*Environ. Res. Lett.*, 15, 034064, <https://doi.org/10.1088/1748-9326/ab70bb>, 2020.](#)

748
749 [Desai, A. R.: Climatic and phenological controls on coherent regional interannual variability of carbon dioxide flux](#)
750 [in a heterogeneous landscape, *J. Geophys. Res.: Biogeosci.*, 115, <https://doi.org/10.1029/2010JG001423>, 2010.](#)

751
752 [Ensminger, I., Sveshnikov, D., Campbell, D. A., Funk, C., Jansson, S., Lloyd, J., Shibistova, O., and Öquist, G.:](#)
753 [Intermittent low temperatures constrain spring recovery of photosynthesis in boreal Scots pine forests, *Global*](#)
754 [Change Biol., 10, 995–1008, <https://doi.org/10.1111/j.1365-2486.2004.00781.x>, 2004.](#)

755 ▼ Deleted: ¶

Deleted: ¶

Deleted: Bloom, A. A., Bowman, K. W., Liu, J., Konings, A. G., Worden, J. R., Parazoo, N. C., Meyer, V., Reager, J. T., Worden, H. M., Jiang, Z., Quetin, G. R., Smallman, T. L., Exbrayat, J.-F., Yin, Y., Saatchi, S. S., Williams, M., and Schimel, D. S.: Lagged effects dominate the inter-annual variability of the 2010–2015 tropical carbon balance, 1–49, <https://doi.org/10.5194/bg-2019-459>, 2020. ¶

Deleted: Agricultural and Forest Meteorology

Field Code Changed

Deleted: ¶

766 Euskirchen, E. S., Carman, T. B., and McGuire, A. D.: Changes in the structure and function of northern Alaskan
767 ecosystems when considering variable leaf-out times across groupings of species in a dynamic vegetation model,
768 *Global Change Biol.*, 20, 963–978, <https://doi.org/10.1111/gcb.12392>, 2014.
769
770 Exbrayat, J.-F., Bloom, A. A., Falloon, P., Ito, A., Smallman, T. L., and Williams, M.: Reliability ensemble
771 averaging of 21st century projections of terrestrial net primary productivity reduces global and regional
772 uncertainties, *Earth Syst. Dynam.*, 9, 153–165, <https://doi.org/10.5194/esd-9-153-2018>, 2018.
773
774 **Famiglietti, C. A., Smallman, T. L., Levine, P. A., Flack-Prain, S., Quetin, G. R., Meyer, V., Parazoo, N. C., Stettz,**
775 **S. G., Yang, Y., Bonal, D., Bloom, A. A., Williams, M., and Konings, A. G.: Optimal model complexity for**
776 **terrestrial carbon cycle prediction, *Biogeosciences*, 18, 2727–2754, <https://doi.org/10.5194/bg-18-2727-2021>, 2021.**
777
778 **Flynn, D. F. B. and Wolkovich, E. M.: Temperature and photoperiod drive spring phenology across all species in a**
779 **temperate forest community, *New Phytol.*, 219, 1353–1362, <https://doi.org/10.1111/nph.15232>, 2018.**
780
781 **Forkel, M., Carvalhais, N., Rödenbeck, C., Keeling, R., Heimann, M., Thonicke, K., Zaehle, S., and Reichstein, M.:**
782 **Enhanced seasonal CO₂ exchange caused by amplified plant productivity in northern ecosystems, *Science*, 351,**
783 **696–699, <https://doi.org/10.1126/science.aac4971>, 2016.**
784
785 **Fox, A., Williams, M., Richardson, A. D., Cameron, D., Gove, J. H., Quaife, T., Ricciuto, D., Reichstein, M.,**
786 **Tomelleri, E., Trudinger, C. M., and Van Wijk, M. T.: The REFLEX project: Comparing different algorithms and**
787 **implementations for the inversion of a terrestrial ecosystem model against eddy covariance data, *Agric. For.***
788 ***Meteorol.*, 149, 1597–1615, <https://doi.org/10.1016/j.agrformet.2009.05.002>, 2009.**
789
790 **Frank, J. M., Massman, W. J., Ewers, B. E., Huckaby, L. S., and Negrón, J. F.: Ecosystem CO₂/H₂O fluxes are**
791 **explained by hydraulically limited gas exchange during tree mortality from spruce bark beetles, *J. Geophys. Res.***
792 ***Biogeosci.*, 119, 1195–1215, <https://doi.org/10.1002/2013JG002597>, 2014.**
793
794 **Goulden, M. and Bales, R.: California forest die-off linked to multi-year deep soil drying in 2012–2015 drought,**
795 ***Nat. Geosci.*, 12, 1, <https://doi.org/10.1038/s41561-019-0388-5>, 2019.**
796
797 **Greenland, D.: The Climate of Niwot Ridge, Front Range, Colorado, U.S.A., *Arct. Alp. Res.*, 21, 380–391,**
798 **<https://doi.org/10.1080/00040851.1989.12002751>, 1989.**
799
800 **Haario, H., Saksman, E., and Tamminen, J.: An Adaptive Metropolis Algorithm, *Bernoulli*, 7, 223–242,**
801 **<https://doi.org/10.2307/3318737>, 2001.**
802
803 **Hu, J., Moore, D. J. P., Burns, S. P., and Monson, R. K.: Longer growing seasons lead to less carbon sequestration**
804 **by a subalpine forest, *Global Change Biol.*, 16, 771–783, <https://doi.org/10.1111/j.1365-2486.2009.01967.x>, 2010.**
805
806 **Huxman, T. E., Turnipseed, A. A., Sparks, J. P., Harley, P. C., and Monson, R. K.: Temperature as a control over**
807 **ecosystem CO₂ fluxes in a high-elevation, subalpine forest, *Oecologia*, 134, 537–546,**
808 **<https://doi.org/10.1007/s00442-002-1131-1>, 2003.**
809
810 **Ishida, A., Nakano, T., Sekikawa, S., Maruta, E., and Masuzawa, T.: Diurnal changes in needle gas exchange in**
811 **alpine *Pinus pumila* during snow-melting and summer seasons, *Ecol. Res.*, 16, 107–116,**
812 **<https://doi.org/10.1046/j.1440-1703.2001.00376.x>, 2001.**
813
814 **Kattge, J. and Knorr, W.: Temperature acclimation in a biochemical model of photosynthesis: a reanalysis of data**
815 **from 36 species, *Plant Cell Environ.*, 30, 1176–1190, <https://doi.org/10.1111/j.1365-3040.2007.01690.x>, 2007.**
816
817 **Keenan, T. F., Davidson, E., Moffat, A. M., Munger, W., and Richardson, A. D.: Using model-data fusion to**
818 **interpret past trends, and quantify uncertainties in future projections, of terrestrial ecosystem carbon cycling, *Global***
819 ***Change Biol.*, 18, 2555–2569, <https://doi.org/10.1111/j.1365-2486.2012.02684.x>, 2012.**
820

Deleted: Famiglietti, C. A., Smallman, T. L., Levine, P. A., Flack-Prain, S., Quetin, G. R., Meyer, V., Parazoo, N. C., Stettz, S. G., Yang, Y., Bonal, D., Bloom, A. A., Williams, M., and Konings, A. G.: Optimal model complexity for terrestrial carbon cycle prediction, *Biogeosciences*, 18, 2727–2754, <https://doi.org/10.5194/bg-18-2727-2021>, 2021.

Deleted: ¶

Deleted: ¶

Deleted: Nature Geoscience

Deleted: ¶
Goulden, M. L., Anderson, R. G., Bales, R. C., Kelly, A. E., Meadows, M., and Winston, G. C.: Evapotranspiration along an elevation gradient in California's Sierra Nevada, 117, <https://doi.org/10.1029/2012JG002027>, 2012. ¶

Deleted: Greenland, D.: The Climate of Niwot Ridge, Front Range, Colorado, U.S.A., 21, 380–391, <https://doi.org/10.1080/00040851.1989.12002751>, 1989. ¶
Haario, H., Saksman, E., and Tamminen, J.: An adaptive Metropolis algorithm, *Bernoulli*, 7, 223–242, 2001.

Deleted: ¶

Deleted: ¶

844 Keenan, T. F., Gray, J., Friedl, M. A., Toomey, M., Bohrer, G., Hollinger, D. Y., Munger, J. W., O’Keefe, J.,
845 Schmid, H. P., Wing, I. S., Yang, B., and Richardson, A. D.: Net carbon uptake has increased through warming-
846 induced changes in temperate forest phenology, *Nat. Clim. Change*, 4, 598–604,
847 <https://doi.org/10.1038/nclimate2253>, 2014.

848
849 Knowles, J. F., Burns, S. P., Blanken, P. D., and Monson, R. K.: Fluxes of energy, water, and carbon dioxide from
850 mountain ecosystems at Niwot Ridge, Colorado, *Plant Ecol. Divers.*, 8, 663–676,
851 <https://doi.org/10.1080/17550874.2014.904950>, 2015.

852
853 Knowles, J. F., Molotch, N. P., Trujillo, E., and Litvak, M. E.: Snowmelt-Driven Trade-Offs Between Early and
854 Late Season Productivity Negatively Impact Forest Carbon Uptake During Drought, *Geophys. Res. Lett.*, 45, 3087–
855 3096, <https://doi.org/10.1002/2017GL076504>, 2018.

856
857 Korzukhin, M. D., Ter-Mikaelian, M. T., and Wagner, R. G.: Process versus empirical models: which approach for
858 forest ecosystem management?, *Can. J. For. Res.*, 26, <https://doi.org/10.1139/x26-096>, 2011.

859
860 **Deleted:** [Lasslop, G., Reichstein, M., Papale, D., Richardson, A. D., Arneth, A., Barr, A., Stoy, P., and Wohlfahrt, G.: Separation of net ecosystem exchange into assimilation and respiration using a light response curve approach: critical issues and global evaluation, *Global Change Biol.*, 16, 187–208, <https://doi.org/10.1111/j.1365-2486.2009.02041.x>, 2009.](#)

861
862
863
864
865 Lin, J. C., Mallia, D. V., Wu, D., and Stephens, B. B.: How can mountaintop CO₂ observations be used to constrain
866 regional carbon fluxes?, *Atmos. Chem. Phys.*, 17, 5561–5581, <https://doi.org/10.5194/acp-17-5561-2017>, 2017.

867
868 López-Blanco, E., Exbrayat, J.-F., Lund, M., Christensen, T. R., Tamstorf, M. P., Slevin, D., Hugelius, G., Bloom,
869 A. A., and Williams, M.: Evaluation of terrestrial pan-Arctic carbon cycling using a data-assimilation system, *Earth*
870 *Syst. Dynam.*, 10, 233–255, <https://doi.org/10.5194/esd-10-233-2019>, 2019.

871
872 **Deleted:** [Mayr, S., Schmid, P., Laur, J., Rosner, S., Charra-Vaskou, K., Dämon, B., and Hacke, U. G.: Uptake of Water via Branches Helps Timberline Conifers Refill Embolized Xylem in Late Winter, *Plant Physiol.*, 164, 1731–1740, <https://doi.org/10.1104/pp.114.236646>, 2014.](#)

873
874
875
876
877 **Deleted:** [Magney, T. S., Bowling, D. R., Logan, B. A., Grossmann, K., Stutz, J., Blanken, P. D., Burns, S. P., Cheng, R., Garcia, M. A., Köhler, P., Lopez, S., Parazoo, N. C., Raczka, B., Schimel, D., and Frankenberg, C.: Mechanistic evidence for tracking the seasonality of photosynthesis with solar-induced fluorescence, *PNAS*, 116, 11640–11645, <https://doi.org/10.1073/pnas.1900278116>, 2019.](#)

878
879
880
881
882 **Deleted:** [Medlyn, B. E., Dreyer, E., Ellsworth, D., Forstreuter, M., Harley, P. C., Kirschbaum, M. U. F., Roux, X. L., Montpied, P., Strassmeyer, J., Walcroft, A., Wang, K., and Loustau, D.: Temperature response of parameters of a biochemically based model of photosynthesis. II. A review of experimental data, *Plant Cell Environ.*, 25, 1167–1179, <https://doi.org/10.1046/j.1365-3040.2002.00891.x>, 2002.](#)

883
884
885
886
887
888
889
890
891
892
893
894
895
896
897
898
899
900
901
902
903
904
905
906
907
908
909
910
911
912
913
914
915
916
917
918
919
920
921
922
923
924
925
926
927
928
929
930
931
932
933
934
935
936
937
938
939
940
941
942
943
944
945
946
947
948
949
950
951
952
953
954
955
956
957
958
959
960
961
962
963
964
965
966
967
968
969
970
971
972
973
974
975
976
977
978
979
980
981
982
983
984
985
986
987
988
989
990
991
992
993
994
995
996
997
998
999
1000

Deleted: [Lasslop, G., Reichstein, M., Papale, D., Richardson, A., Arneth, A., Barr, A., Stoy, P., and Wohlfahrt, G.: Separation of net ecosystem exchange into assimilation and respiration using a light response curve approach: critical issues and global evaluation, 16, 2009.](#)

Deleted: [Magney, T. S., Bowling, D. R., Logan, B. A., Grossmann, K., Stutz, J., Blanken, P. D., Burns, S. P., Cheng, R., Garcia, M. A., Köhler, P., Lopez, S., Parazoo, N. C., Raczka, B., Schimel, D., and Frankenberg, C.: Mechanistic evidence for tracking the seasonality of photosynthesis with solar-induced fluorescence, PNAS, 116, 11640–11645, <https://doi.org/10.1073/pnas.1900278116>, 2019.](#)

Deleted: [cultural](#)

Deleted: [and](#)

Deleted: [est](#)

Deleted: [ogy](#)

Deleted: [cultural](#)

920
921 [Parazoo, N. C., Magney, T., Norton, A., Raczka, B., Bacour, C., Maignan, F., Baker, I., Zhang, Y., Qiu, B., Shi, M.,](#)
922 [MacBean, N., Bowling, D. R., Burns, S. P., Blanken, P. D., Stutz, J., Grossmann, K., and Frankenberg, C.: Wide](#)
923 [discrepancies in the magnitude and direction of modeled solar-induced chlorophyll fluorescence in response to light](#)
924 [conditions. *Biogeosciences*, 17, 3733–3755, <https://doi.org/10.5194/bg-17-3733-2020>, 2020.](#)
925
926 [Pierrat, Z., Nehemy, M. F., Roy, A., Magney, T., Parazoo, N. C., Laroque, C., Pappas, C., Sonnentag, O.,](#)
927 [Grossmann, K., Bowling, D. R., Seibt, U., Ramirez, A., Johnson, B., Helgason, W., Barr, A., and Stutz, J.: Tower-](#)
928 [Based Remote Sensing Reveals Mechanisms Behind a Two-phased Spring Transition in a Mixed-Species Boreal](#)
929 [Forest, *J. Geophys. Res.: Biogeosci.*, 126, <https://doi.org/10.1029/2020JG006191>, 2021.](#)
930
931 [Quetin, G. R., Bloom, A. A., Bowman, K. W., and Konings, A. G.: Carbon Flux Variability From a Relatively](#)
932 [Simple Ecosystem Model With Assimilated Data Is Consistent With Terrestrial Biosphere Model Estimates, *J. Adv.*](#)
933 [Model. Earth Syst., 12, <https://doi.org/10.1029/2019MS001889>, 2020.](#)
934
935 [Randerson, J. T., Field, C. B., Fung, I. Y., and Tans, P. P.: Increases in early season ecosystem uptake explain recent](#)
936 [changes in the seasonal cycle of atmospheric CO₂ at high northern latitudes, *Geophys. Res. Lett.*, 26, 2765–2768,](#)
937 [https://doi.org/10.1029/1999GL900500, 1999.](#)
938
939 [Raupach, M. R., Rayner, P. J., Barrett, D. J., DeFries, R. S., Heimann, M., Ojima, D. S., Quegan, S., and](#)
940 [Schmullius, C. C.: Model–data synthesis in terrestrial carbon observation: methods, data requirements and data](#)
941 [uncertainty specifications, *Global Change Biol.*, 11, 378–397, <https://doi.org/10.1111/j.1365-2486.2005.00917.x>,](#)
942 [2005.](#)
943
944 [Reichstein, M., Falge, E., Baldocchi, D., Papale, D., Aubinet, M., Berbigier, P., Bernhofer, C., Buchmann, N.,](#)
945 [Gillmanov, T., Granier, A., Grünwald, T., Havránková, K., Ilvesniemi, H., Janous, D., Knohl, A., Laurila, T., Lohila,](#)
946 [A., Loustau, D., Matteucci, G., Meyers, T., Miglietta, F., Ourcival, J.-M., Pumpanen, J., Rambal, S., Rotenberg, E.,](#)
947 [Sanz, M., Tenhunen, J., Seufert, G., Vaccari, F., Vesala, T., Yakir, D., and Valentini, R.: On the separation of net](#)
948 [ecosystem exchange into assimilation and ecosystem respiration: review and improved algorithm, *Global Change*](#)
949 [Biol., 11, 1424–1439, <https://doi.org/10.1111/j.1365-2486.2005.001002.x>, 2005.](#)
950
951 [Richardson, A. D., Williams, M., Hollinger, D. Y., Moore, D. J. P., Dail, D. B., Davidson, E. A., Scott, N. A.,](#)
952 [Evans, R. S., Hughes, H., Lee, J. T., Rodrigues, C., and Savage, K.: Estimating parameters of a forest ecosystem C](#)
953 [model with measurements of stocks and fluxes as joint constraints, *Oecologia*, 164, 25–40,](#)
954 [https://doi.org/10.1007/s00442-010-1628-y, 2010.](#)
955
956 [Rowland, L., Hill, T. C., Stahl, C., Siebicke, L., Burban, B., Zaragoza-Castells, J., Ponton, S., Bonal, D., Meir, P.,](#)
957 [and Williams, M.: Evidence for strong seasonality in the carbon storage and carbon use efficiency of an Amazonian](#)
958 [forest, *Global Change Biol.*, 20, 979–991, <https://doi.org/10.1111/gcb.12375>, 2014.](#)
959
960 [Schimel, D., Schneider, F. D., and JPL Carbon and Ecosystem Participants: Flux towers in the sky: global ecology](#)
961 [from space, *New Phytol.*, 224, 570–584, <https://doi.org/10.1111/nph.15934>, 2019.](#)
962
963 [Scott-Denton, L. E., Moore, D. J. P., Rosenbloom, N. A., Kittel, T. G. F., Burns, S. P., Schimel, D. S., and Monson,](#)
964 [R. K.: Forecasting net ecosystem CO₂ exchange in a subalpine forest using model data assimilation combined with](#)
965 [simulated climate and weather generation, *J. Geophys. Res. G: Biogeosci.*, 118, 549–565,](#)
966 [https://doi.org/10.1002/jgrg.20039, 2013.](#)
967
968 [Sippel, S., Forkel, M., Rammig, A., Thonicke, K., Flach, M., Heimann, M., Otto, F. E. L., Reichstein, M., and](#)
969 [Mahecha, M. D.: Contrasting and interacting changes in simulated spring and summer carbon cycle extremes in](#)
970 [European ecosystems, *Environ. Res. Lett.*, 12, 075006, <https://doi.org/10.1088/1748-9326/aa7398>, 2017.](#)
971
972 [Smallman, T. L., Exbrayat, J.-F., Mencuccini, M., Bloom, A. A., and Williams, M.: Assimilation of repeated woody](#)
973 [biomass observations constrains decadal ecosystem carbon cycle uncertainty in aggrading forests, *J. Geophys. Res.*](#)
974 [G: Biogeosci., 122, 528–545, <https://doi.org/10.1002/2016JG003520>, 2017.](#)
975

Deleted: Parazoo, N. C., Magney, T., Norton, A., Raczka, B., Bacour, C., Maignan, F., Baker, I., Zhang, Y., Qiu, B., Shi, M., MacBean, N., Bowling, D. R., Burns, S. P., Blanken, P. D., Stutz, J., Grossman, K., and Frankenberg, C.: Wide Discrepancies in the Magnitude and Direction of Modelled SIF in Response to Light Conditions, 2020, 1–42, <https://doi.org/10.5194/bg-2019-508>, 2020.*

Deleted: e2019MS001889,

Deleted: ogist

985 Smith, W. K., Fox, A. M., MacBean, N., Moore, D. J. P., and Parazoo, N. C.: Constraining estimates of terrestrial
986 carbon uptake: new opportunities using long-term satellite observations and data assimilation, *New Phytol.*, 225,
987 105–112, <https://doi.org/10.1111/nph.16055>, 2020.

988

989 Stavros, E. N., Schimel, D., Pavlick, R., Serbin, S., Swann, A., Duncanson, L., Fisher, J. B., Fasnacht, F., Ustin, S.,
990 Dubayah, R., Schweiger, A., and Wennberg, P.: ISS observations offer insights into plant function, *Nat. Ecol. Evol.*,
991 1, 1–5, <https://doi.org/10.1038/s41559-017-0194>, 2017.

992

993 [Stinziano, J. R. and Way, D. A.: Autumn photosynthetic decline and growth cessation in seedlings of white spruce
994 are decoupled under warming and photoperiod manipulations. *Plant Cell Environ.*, 40, 1296–1316,
995 <https://doi.org/10.1111/pce.12917>, 2017.](https://doi.org/10.1111/pce.12917)

996

997 [Stinziano, J. R., Hüner, N. P. A., and Way, D. A.: Warming delays autumn declines in photosynthetic capacity in a
998 boreal conifer, Norway spruce \(*Picea abies*\). *Tree Physiol.*, 35, 1303–1313, <https://doi.org/10.1093/treephys/tpv118>,
999 2015.](https://doi.org/10.1093/treephys/tpv118)

1000

1001 Sun, Y., Frankenberg, C., Wood, J. D., Schimel, D. S., Jung, M., Guanter, L., Drewry, D. T., Verma, M., Porcar-
1002 Castell, A., Griffis, T. J., Gu, L., Magney, T. S., Köhler, P., Evans, B., and Yuen, K.: OCO-2 advances
1003 photosynthesis observation from space via solar-induced chlorophyll fluorescence, *Science*, 358,
1004 <https://doi.org/10.1126/science.aam5747>, 2017.

1005

1006 [Tanja, S., Berninger, F., Vesala, T., Markkanen, T., Hari, P., Mäkelä, A., Ilvesniemi, H., Hänninen, H., Nikinmaa,
1007 E., Huttula, T., Laurila, T., Aurela, M., Grelle, A., Lindroth, A., Arneeth, A., Shibistova, O., and Lloyd, J.: Air
1008 temperature triggers the recovery of evergreen boreal forest photosynthesis in spring, *Global Change Biol.*, 9, 1410–
1009 1426, <https://doi.org/10.1046/j.1365-2486.2003.00597.x>, 2003.](https://doi.org/10.1046/j.1365-2486.2003.00597.x)

1010

1011 Thurner, M., Beer, C., Santoro, M., Carvalhais, N., Wutzler, T., Schepaschenko, D., Shvidenko, A., Kompter, E.,
1012 Ahrens, B., Levick, S. R., and Schmillius, C.: Carbon stock and density of northern boreal and temperate forests,
1013 *Global Change Biol.*, 23, 297–310, <https://doi.org/10.1111/geb.12125>, 2014.

1014

1015 Turnipseed, A. A., Blanken, P. D., Anderson, D. E., and Monson, R. K.: Energy budget above a high-elevation
1016 subalpine forest in complex topography, *Agric. For. Meteorol.*, 110, 177–201, [https://doi.org/10.1016/S0168-
1017 1923\(01\)00290-8](https://doi.org/10.1016/S0168-1923(01)00290-8), 2002.

1018

1019 Turnipseed, A. A., Anderson, D. E., Burns, S., Blanken, P. D., and Monson, R. K.: Airflows and turbulent flux
1020 measurements in mountainous terrain: Part 2: Mesoscale effects, *Agric. For. Meteorol.*, 125, 187–205,
1021 <https://doi.org/10.1016/j.agrformet.2004.04.007>, 2004.

1022

1023 Wang, Y.-P., Trudinger, C. M., and Enting, I. G.: A review of applications of model–data fusion to studies of
1024 terrestrial carbon fluxes at different scales, *Agric. For. Meteorol.*, 149, 1829–1842,
1025 <https://doi.org/10.1016/j.agrformet.2009.07.009>, 2009.

1026

1027 Williams, M., Rastetter, E. B., Fernandes, D. N., Goulden, M. L., Wofsy, S. C., Shaver, G. R., Melillo, J. M.,
1028 Munger, J. W., Fan, S.-M., and Nadelhoffer, K. J.: Modelling the soil–plant–atmosphere continuum in a *Quercus*–
1029 *Acer* stand at Harvard Forest: the regulation of stomatal conductance by light, nitrogen and soil/plant hydraulic
1030 properties, *Plant Cell Environ.*, 19, 911–927, <https://doi.org/10.1111/j.1365-3040.1996.tb00456.x>, 1996.

1031

1032 Williams, M., Rastetter, E. B., Fernandes, D. N., Goulden, M. L., Shaver, G. R., and Johnson, L. C.: Predicting
1033 Gross Primary Productivity in Terrestrial Ecosystems, *Ecol. Appl.*, 7, 882–894, [https://doi.org/10.1890/1051-
1034 0761\(1997\)007\[0882:PGPPIT\]2.0.CO;2](https://doi.org/10.1890/1051-0761(1997)007[0882:PGPPIT]2.0.CO;2), 1997.

1035

1036 Williams, M., Law, B. E., Anthoni, P. M., and Unsworth, M. H.: Use of a simulation model and ecosystem flux data
1037 to examine carbon–water interactions in ponderosa pine, *Tree Physiol.*, 21, 287–298,
1038 <https://doi.org/10.1093/treephys/21.5.287>, 2001.

1039

Deleted: ultural and

Deleted: Forest

Deleted: Meteorology

Deleted: ultural and

Deleted: Forest

Deleted: Meteorology

Deleted: Agricultural

Deleted: and

Deleted: est

Deleted: Meteorology

Deleted: Physiology

1051 Williams, M., Schwarz, P. A., Law, B. E., Irvine, J., and Kurpius, M. R.: An improved analysis of forest carbon
1052 dynamics using data assimilation, *Global Change Biol.*, 11, 89–105, <https://doi.org/10.1111/j.1365->
1053 [2486.2004.00891.x](https://doi.org/10.1111/j.1365-2486.2004.00891.x), 2005.

1054

1055 Williams, M. W., Seastedt, T. R., Bowman, W. D., McKnight, D. M., and Suding, K. N.: An overview of research
1056 from a high elevation landscape: the Niwot Ridge, Colorado Long Term Ecological Research programme, *Plant*
1057 *Ecolog. Divers.*, 8, 597–605, <https://doi.org/10.1080/17550874.2015.1123320>, 2015.

1058

1059 Winchell, T. S., Barnard, D. M., Monson, R. K., Burns, S. P., and Molotch, N. P.: Earlier snowmelt reduces
1060 atmospheric carbon uptake in midlatitude subalpine forests, *Geophys. Res. Lett.*, 43, 8160–8168,
1061 <https://doi.org/10.1002/2016GL069769>, 2016.

1062

1063 [Wolf, S., Keenan, T. F., Fisher, J. B., Baldocchi, D. D., Desai, A. R., Richardson, A. D., Scott, R. L., Law, B. E.,](https://doi.org/10.1073/pnas.1519620113)
1064 [Litvak, M. E., Brunsell, N. A., Peters, W., and van der Laan-Luijkx, I. T.: Warm spring reduced carbon cycle impact](https://doi.org/10.1073/pnas.1519620113)
1065 [of the 2012 US summer drought, PNAS, 113, 5880, https://doi.org/10.1073/pnas.1519620113, 2016.](https://doi.org/10.1073/pnas.1519620113)

1066

1067 ▼ Wutzler, T., Lucas-Moffat, A., Migliavacca, M., Knauer, J., Sickel, K., Šigut, L., Menzer, O., and Reichstein, M.:
1068 Basic and extensible post-processing of eddy covariance flux data with REddyProc, *Biogeosciences*, 15, 5015–5030,
1069 <https://doi.org/10.5194/bg-15-5015-2018>, 2018.

1070

1071 ▼ Xu, C., Liu, H., Williams, A. P., Yin, Y., and Wu, X.: Trends toward an earlier peak of the growing season in
1072 Northern Hemisphere mid-latitudes, *Global Change Biol.*, 22, 2852–2860, <https://doi.org/10.1111/gcb.13224>, 2016.

1073

1074 [Yang, Q., Blanco, N. E., Hermida-Carrera, C., Lehotaj, N., Hurry, V., and Strand, Å.: Two dominant boreal conifers](https://doi.org/10.1038/s41467-019-13954-0)
1075 [use contrasting mechanisms to reactivate photosynthesis in the spring, Nat Commun, 11, 128,](https://doi.org/10.1038/s41467-019-13954-0)
1076 [https://doi.org/10.1038/s41467-019-13954-0, 2020.](https://doi.org/10.1038/s41467-019-13954-0)

1077

1078 ▼ Yin, Y., Bloom, A. A., Worden, J., Saatchi, S., Yang, Y., Williams, M., Liu, J., Jiang, Z., Worden, H., Bowman, K.,
1079 Frankenberg, C., and Schimel, D.: Fire decline in dry tropical ecosystems enhances decadal land carbon sink, *Nat*
1080 *Commun*, 11, 1900, <https://doi.org/10.1038/s41467-020-15852-2>, 2020.

1081

Deleted: ¶

Deleted: ¶

Deleted: ¶
Wolf, S., Keenan, T. F., Fisher, J. B., Baldocchi, D. D.,
Desai, A. R., Richardson, A. D., Scott, R. L., Law, B. E.,
Litvak, M. E., Brunsell, N. A., Peters, W., and van der Laan-
Luijkx, I. T.: Warm spring reduced carbon cycle impact of
the 2012 US summer drought, *Proc Natl Acad Sci USA*, 113,
5880, <https://doi.org/10.1073/pnas.1519620113>, 2016.¶

Deleted: ¶